Plasmonic Gold Nanostructures for Biodiagnostics and Photothermal Therapeutics

By

Eden Pauline Roshan Paul

Thesis

Submitted to the Faculty of the
Graduate School of Vanderbilt University
in partial fulfillment of the requirements
for the degree of

MASTER OF SCIENCE
in
Chemical Engineering

May 10, 2019
Nashville Tennessee

Approved:
Rizia Bardhan, PhD
Marjan Rafat, PhD

TABLE OF CONTENTS

LIST OF FIGURES

Figure

CHAPTER 1

INTRODUCTION

1.1 Motivation

Cardiovascular disease and cancer are the two leading causes of death worldwide.[1] In fact, some people who have been treated for breast cancer or lymphoma have a higher risk of developing congestive heart failure than people who have not had cancer.[2] Congestive heart failure is a condition in which damaged or weakened heart muscles can no longer effectively pump blood to the rest of the body. Heart disease, high blood pressure, and diabetes are all risks for heart failure, as are certain cancer treatments such as chemotherapy, radiation, immunotherapy, as well as some targeted therapies.[3] This calls for new and innovative treatments and diagnostic techniques, with enhanced efficacy and safety, for cancer and heart failure, on an individual patient basis. Nanotechnologies exhibit a scientific advance that have the potential to revolutionize multiple areas of medicine and biology, especially in the field of biodiagnostics and cancer treatments. There has been an accelerated interest in nanotechnology applications in medicine in attempts to prevent and treat human diseases.[4] The field of nanomedicine, a subset of nanotechnology that refers to highly specific medical intervention at the molecular scale, has displayed great promise for millions of patients for more efficient and cost-friendly healthcare. Nanoparticle-based therapies in particular have showed tremendous capacities for medical purposes, ranging between diagnosing diseases to providing new therapies.[5] However, in order to remain clinically relevant, current nanoparticle-based technologies need to overcome several challenges that include potential cytotoxicity, selective particle delivery, imaging of nanoparticles, as well as real-time assessment of therapeutic efficacy.

Gold nanoparticles (AuNPs) have been utilized for the treatment of rheumatoid arthritis, while tremendous research is being concurrently conducted to reveal the potential antimicrobial, anti-cancer, and biodiagnostic applications of AuNPs for clinical settings.[6] AuNPs have significant applications in the field of biomedicine due to (i) their chemical stability, making them less hazardous, (ii) their biocompatibility and lack of interference with other potentially labeled materials such as antibodies and other biomarkers, and (iii) their straightforward fabrication and synthesis process.[7] Another favorable characteristic of AuNPs is the capacity to tune their size, shape, and surface properties to suit specific biological applications.[8] For example, plasmonic AuNPs have the ability to be tuned to absorb near-infrared light, which penetrates tissue more deeply than other wavelengths, and can efficiently convert this light to heat for the purpose of photothermal therapy (PTT).[9] The strong electromagnetic fields of these plasmonic AuNPs also enhance the signal of Raman spectroscopy, allowing sensitive molecular imaging and detection both *in vitro* and *in vivo*.[10] As such, AuNPs are advantageous for cancer therapy and imaging applications. There are two different types of AuNPs that are involved in my projects. Firstly, there exist previously synthesized multibranched gold nanoantennas (MGNs) or nanostars. To allow for their biocompatibility and use in biodiagnostic applications, they are required to have further surface functionalization as well as appropriate characterization. In order to exploit the light-to-heat conversion property of AuNPs, the synthesis of gold-coated liposomes that have the potential to encapsulate chemotherapeutic or immunotherapeutic agents which will be released at mild hyperthermia conditions has been attempted. The objective was to engineer AuNPs for surface enhanced Raman spectroscopy (SERS) in order to provide detailed tumor footprints and utilize the same particles for combination therapies (such as chemo-photothermal and immune-photothermal therapies) to treat cancer. With these engineered designs and subsequent AuNP functionalization,

the nanoparticles are capable of providing detailed molecular information of the tumor as well as delivering potent anticancer therapies.

1.2 Cancer Biology

According to the WHO, out of 14.1 million new cancer cases in 2012, there were 8.2 million deaths.[11] While cardiovascular disease remains the leading cause of non-communicable diseases, cancer follows up as a close second.[12] Cancer results from the abnormal proliferation of different kinds of cells in the body, and thus there are more than a hundred different types of cancer, which substantially vary in their response and behavior to treatment. A tumor, or mass of cells, formed of these abnormal cells may remain within the tissue in which it originated (called in situ cancer), or it may begin to invade nearby the original tumor site (called invasive cancer). Invasive tumors are often malignant and when the cells shed into the blood or lymph, the establishment of new tumors (metastases) throughout the body becomes possible.[13] Two categories of genes play roles in triggering cancer. When existing in their normal forms, the genes control the cell cycle, the sequence of events by which cells enlarge and divide. The first category of genes, proto-oncogenes, encourages cell division. The second category, tumor suppressor genes, inhibits cell division. Mutated proto-oncogenes become oncogenes that stimulate excessive division. Mutations in tumor suppressor genes inactivate them, eliminating the critical inhibition of cell division that prevents excessive and uncontrolled growth.[14] This genomic instability serves as the foundation for the "hallmarks of cancer".[15] The hallmarks constitute an organizing principle for rationalizing the complexities of the disease, and comprises of six biological capabilities acquired during the multistep development of human tumors. They include, (a) proliferative signaling, (b) evading growth suppressors, (c) resisting cell death, (d) enabling replicative immortality, (e) inducing angiogenesis, and (f) activating invasion and metastasis.[16]

Research progress in the last two decades has contributed to understanding the listed characteristics with the addition of two new hallmarks – reprograming of energy metabolism, and evading immune destruction.[15] The recognition of the widespread understanding of the above hallmarks will tremendously affect the development of new methods to treat cancer. In order to avoid the spreading of cancer, early detection and treatment is necessary. With the platform proposed in my project, the approach will likely increase cancer detection accuracy and sensitivity. The technology for the purpose of identifying cancer cells in vivo using SERS relies heavily on receptor detection. Thus, the expression and concentration of the proteins of interest will be the most important biological indicators to improve SERS detection. Proteins attached to the surface of cells, called receptors, can provide necessary information in determining the presence of tumor tendencies.[17] The technology depends on detection of these expressed biomarkers, and so the identification of these receptors is very important. Cancer is known to have uncontrollable rates of cell cycles as well as protein synthesis, which translates to the overexpression of biomarkers/receptors of interest on the cell surface, and this can be used for the early detection of the disease.[17]

1.3 Plasmonic Properties of Gold Nanostars

The optical properties of AuNPs originate from their unique interaction with light resulting in their collective coherent oscillation of their free conduction band electrons, or their localized surface plasmon resonance (LSPR).[18] The oscillation of the free electrons decays via two processes:

(a) radiative decay resulting in the very strong visible scattering of light, and (2) nonradiative decay resulting in the conversion of photon energy to thermal energy.[18] The first decay mechanism has been readily utilized in biodiagnostic and imaging. Raman spectroscopy is a technique that provides details about the vibrational modes in a system. The technique is based on the inelastic

scattering of photons, typically from monochromatic (i.e. laser) light. The energy difference between the incident light and the Raman scattered light is indicative of the energy of a molecular vibration.[19] Raman scattering is a very inefficient process, which results in a low detection sensitivity.[20] In order to overcome the weak signals, plasmonic nanostructures like Au and Ag have been utilized.[21] Signal enhancement occurs when a molecule is located within the near field of the nanostructures LSPR and can result in up to 10^{14} enhancement compared to traditional Raman scattering.[22] SERS Raman reporters in conjunction with metal nanostructures have also been heavily used in biological applications. Reporters are active dyes with distinct Raman vibrational bands that can be detected in complex solution matrices. This allows for multiple targets to be identified at once.[23] The projects here examine gold nanostars (GNS) as the detection imaging probe when used in a portable and reusable sandwich biodiagnostic assay.

1.4 Surface Enhanced Raman Spectroscopy, Photothermal Therapy, and Hyperthermia

Optical imaging techniques such as SERS have become popular in the field of biodiagnostics where the optical selectivity is used for better biomarker discrimination.[24] SERS utilizes the enhanced Raman scattering by bringing a Raman-active molecule close to a metal surface, which in our case will be the gold nanostars.[25] As a result of this, an enhancement factor of 10^{9}-10^{12} of the Raman signals can be achieved.[26] Consequently, SERS is an existing technique in the biomedical field that allows for very sensitive detection of molecules, as well as easy distinguishing based on the fingerprint spectrum.[27] SERS enables several advantages when compared to more conventional labeling techniques because of their structure sensitivity as well as the absence of photodecomposition.[28] AuNPs in particular have been extensively studied as potential SERS agents for cancer diagnosis.[29] The SERS imaging technique relies heavily on the enhancement factor of the nanoparticle's Raman signal by generating local high electric fields;

the sharp tips on gold nanostars allow for high electric fields to be generated upon irradiation. The same sharp tips also make gold nanostars efficient carriers of the Raman-active molecules and enables for detection down to pM concentrations.[30] *In vitro* applications of SERS imaging using nanostars have been demonstrated for the study of cellular pathways, detection of specific cells in histology sections, and intracellular pH sensing.[31] Gold nanoparticles (AuNPs) have been widely studied for their localized surface plasmon resonance, or LSPR. LSPR is the collective oscillation of the electron cloud upon light stimulation at the characteristic plasmon resonance of the AuNPs.[25] LSPR can generate a strong enhancement of electromagnetic signals. Following the absorption of light, the plasmon energy must decay through a series of relaxation events and eventually release the energy as either light scattering (radiative relaxation) or heat transfer (non-radiative relaxation) to the surroundings.[32] While the heating of the AuNPs is rapid and in a non-equilibrium state, the cooling occurs via the quasiequilibrium processes of electron-electron scattering, electron-phonon coupling, and phonon-phonon coupling during which heat is dissipated and transferred into the surrounding medium.[33] The photothermal ability, or their effective light-to-heat conversion, of AuNPs has been widely utilized in PTT, in which the heat harvested from the particles can induce cell death and tumor shrinkage.[25]

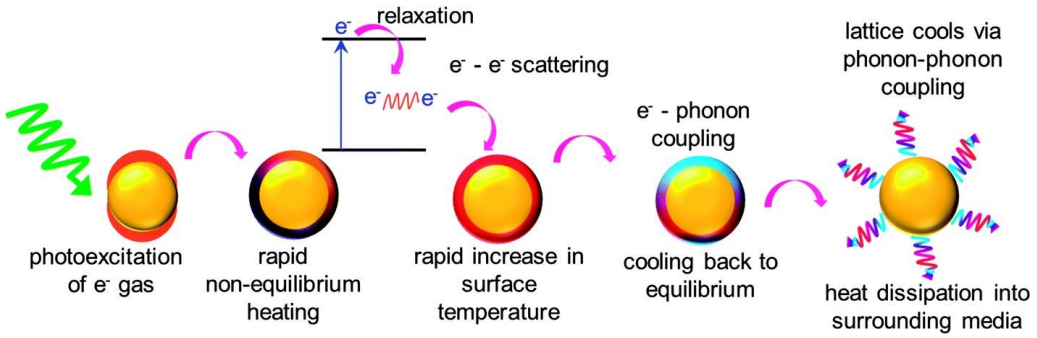

Figure 1.1. Light to heat conversation mechanisms of plasmonic nanoparticles.

Heat as a curative modality has been explored in cancer therapies by many.[34] Hyperthermia refers to small temperature rises, usually 40-45 ºC, initiating a series of subcellular events that render cells susceptible to various forms of damage including apoptosis and eventually cell death.[34] Other effects that are often associated with hyperthermia include the activation of immunological responses and the enhancement of tumor blood flow and oxygenation via greater vascular perfusion and permeability.[34] Hyperthermia can also be used to chemosensitize cancer cells, however this depends largely on the concentration of drug, the tumor type, the increase in tumor temperature, and the time differential between the delivery of chemotherapy and heat.[35] However, current clinical approaches to induce local hyperthermia can be invasive, requiring a heating probe directly in contact with solid tumors (e.g. radiofrequency ablation)[36, 37]. As a result, an innovative, non- invasive hyperthermia method is in demand.

1.5 Plasmonic SERS substrates for Biomolecular Detection

In the past two decades, engineers and scientists alike are beginning to understand the importance of sensing technology with regards to the field of medicine. Some groups have developed techniques that utilize a variety of substrates, for the purpose of designing plasmonic nanostructure diagnostic probes that would be used with handheld Raman instruments.[38] Most of these substrates are cheap, flexible, and robust, in order to be used readily in the field.[39] These advantages of the substrates make for point-of-care, easily accessible, and often disposable diagnostic devices.

Since the dawn of SERS technology, the applications of new sensing tool seem endless. Research groups have worked towards the development of SERS systems that are capable of detecting very low concentrations of target molecules that may serve as indicators for the early onset of a disease. SERS also allows for multiplexed detection, because of the distinct and narrow

peak-widths in the resulting spectra; the multiplex capacity is what allows one to track and trace multiple target molecules of interest at the same time.[40] Wu et al. designed a half-sandwich assay where the capture and detection probes were gold and silver nanorods on glass substrates for the multiplexed detection transcription factors p53 and p21 for early cancer detection.[41] Another group performed a similar assay on a glass substrate coated in gold nanotriangles for the detection of human immunoglobulin G (IgG) at low concentrations; their device had a limit of detection at 0.5 pg/mL.[42] In this project, a PDMS-glass microfluidic chip serves as the substrate for a full sandwich assay, where magnetic microbeads coated in anti-cardiac troponin I antibody are the capture probes and Raman reporter (5,5′-Dithiobis(2-nitrobenzoic acid), DTNB) and cardiac troponin I peptide P2 tagged gold nanostars are the sensitive detection probes. The target molecule, cardiac troponin I is sandwiched between the two, and the gold nanostars on top of the assay provide extremely high near-field enhancements. It is expected that with this technology, the development of an ultrasensitive biodiagnostic tool for the detection of the cardiac biomarker will be possible especially with the use of the multiple targeted ligand, anti-cardiac troponin I.

CHAPTER 2

GOLD NANOSTARS FOR ULTRASENSITIVE AND MULTIPLEXED BIODIAGNOSTICS: PRADA, *P*ORTABLE *R*EUSABLE *A*CCURATE *D*IAGNOSTICS WITH NANO*A*NTENNAS FOR MULTIPLEXED BIOMARKER SCREENING

2.1 Summary

Precise monitoring of specific biomarkers in biological fluids with accurate biodiagnostic sensors is critical for early diagnosis of diseases and subsequent treatment planning. In this work we demonstrate an innovative biodiagnostic sensor, PRADA: ***p***ortable ***r***eusable ***a***ccurate ***d***iagnostics with nano***a***ntennas, for multiplexed biomarker detection in small volumes (~50 µL) enabled in a microfluidic platform. In the PRADA platform, magnetic microbeads capture cardiac troponin I (cTnI), a well-accepted biomarker of cardiac disorders, and gold nanostar "antennas" labeled with peptide recognition elements and Raman reporters to detect the biomarkers via surface-enhanced Raman spectroscopy (SERS) in both buffer and de-identified human serum samples. The nanostar/peptide conjugates are leveraged to achieve high sensitivity, with a limit of detection of 30 pg/mL of cTnI. Moreover, the magnetic beads enabled regeneration and reuse of PRADA for over 15 cycles with the same sensor chip. Further, the narrow linewidths of SERS enabled multiplexed detection of cTnI and neuropeptide Y (NPY), a biomarker of stress and cognition, in both buffer and human serum with high sensitivity and specificity. In summary, versatile and reusable PRADA will ultimately enable rapid and low-cost assessment of multiple biomarkers in clinical samples amenable to resource-limited settings.

2.2 Introduction

Rapid and accurate detection of disease-specific biomarkers is imperative for monitoring human health during the course of a disease, for treatment planning, and for post-treatment

response.[43, 44] Enzyme-linked immunosorbent assays (ELISAs) and mass spectrometry are the current clinical standard for biomarker evaluation of clinical samples. Whereas these workhorses of clinical laboratories give rise to accurate diagnostics, the long sample prep time, high operational cost, large sample volumes required, and low speed of analyses limit the utility of these techniques for early and rapid detection.[45] This has motivated the development of a broad array of biodiagnostic sensors using various readout signals (e.g. colorimetry, electrochemistry, surface plasmon resonance, Raman, and fluorescence) to overcome the limitations of these current techniques.[46-51] For clinical applications, biodiagnostic devices must rigorously meet the following functions: *(i)* multiplexed detection of biomarkers enabling accurate and quantitative bioanalysis at clinically- relevant levels; *(ii)* straightforward sample preparation and rapid real-time readout times; *(iii)* portable and low sample consumption for translation to resource-limited settings; *(iv)* prolonged reagent shelf life and stability; and *(v)* ability to regenerate and reuse, thereby lowering the overall cost of the sensors.[52, 53]

In this work we have designed a new paradigm of biodiagnostic sensor, PRADA, which synergistically integrates all of these functionalities allowing multiplexed detection of biomarkers in human serum at clinically relevant levels. PRADA, ***p***ortable ***r***eusable ***a***ccurate ***d***iagnostics with nano***a***ntennas, is a sandwich immunoassay (Fig. 2.1) with polyclonal antibody (pAbs) functionalized magnetic microbeads to capture the biomarkers. Near-infrared resonant gold nanostar (GNS) “antennas” labeled with Raman reporters and short peptide recognition elements detect the biomarkers via SERS. SERS is an exciting immunodetection technique due to its exceptional sensitivity, specificity, and multiplexing ability with minimal spectral overlap from Raman reporter molecules.[54-57] The antenna-like behavior of GNSs is attributable to their unique geometry, as seen in Figure 2.2b, where the spherical core acts as an antenna absorbing near-

infrared light and the branches behave as emitters localizing the absorbed light at the tips enabling intense electric fields.[58-60] We have shown the near-field electromagnetic radiation generated at the protrusions of GNSs give rise to a ~10^9 enhancement in SERS signal, resulting in ultrasensitive detection.[61, 62] We used PRADA to detect cardiac troponin I (cTnI), a well-accepted serum biomarker of myocardial infarction, stress, and ischemic stroke.[63, 64] cTnI is routinely assessed in patient samples in clinical laboratories to detect myocardial damage, with a clinical range for at-risk patients of 0.1-10 ng/mL.[64] Here, ultrasensitive PRADA has shown a limit of detection (LOD) of 0.03 ng/mL of cTnI in both buffer and human serum ideal for risk stratification. The high sensitivity and specificity of PRADA is due to the GNSs/peptide conjugates. Short peptides represent an attractive alternative to monoclonal Abs due to their low cost, high shelf life, and stability.[65, 66] Further, peptides are significantly smaller in size than antibodies, causing closer proximity to the GNSs and thereby allowing better coupling of the nanostars with the electromagnetic fields of the antennas and resulting in high accuracy. We also demonstrated multiplexed detection of cTnI and neuropeptide Y (NPY) in human serum, achieving a highly sensitive detection range of 0.05 pg/mL for both biomarkers. NPY is abundant in the human brain, and depleted plasma NPY concentration has been correlated with stress, anxiety, fatigue, and post-traumatic stress disorder at a clinically relevant level of <1.5ng/mL.[67-69] We also translated PRADA to a simple microfluidic device enabling multiplexing in small sample volumes (~50 µL) with rapid readout times and the ability to reuse the same device over multiple cycles.[70, 71]

We envision cutting-edge PRADA will ultimately enable early, accurate, and multiplexed detection of a range of biomolecules including proteins, cytokines, chemokines among others at clinically relevant levels to allow rapid clinical decision of an optimum treatment strategy. The reusability of PRADA and ability to detect with high sensitivity in low sample volumes will lower

the overall costs amenable to resource-limited setting. Further, the biomarkers studied here, cTnI and NPY, are relevant to the physiological and psychological health of military personnel.[72, 73] Therefore PRADA will be of particular utility to physicians in resource limited settings for rapid risk prediction and accurate treatment plan for affected individuals.

2.3 Results and Discussion

The design of PRADA with magnetic microbead capture probes and GNS "antennas" as detection probes is demonstrated in Figure 2.1. In this design, polyclonal antibody (pAb) functionalized magnetic microbead capture probes are assembled onto passivated glass slides with a magnet to form a uniform layer. These capture probes are then incubated with buffer or serum solutions with the desired antigen that facilitates the microbeads to capture the relevant biomarkers via the pAbs. Next, GNSs labeled with a Raman reporter and small peptides are introduced and bind to different receptors on the biomarkers, completing the sandwich immunocomplex. After magnetic separation of unbound antigen, a near-infrared laser excites the Raman reporter molecules on GNSs and the SERS signal is measured for quantitative evaluation of the antigen present in serum or buffer. Here we first demonstrated the targeted detection of a single biomarker of myocardial infarction, cardiac troponin I (cTnI), followed by multiplexed detection of both cTnI and neuropeptide Y (NPY).

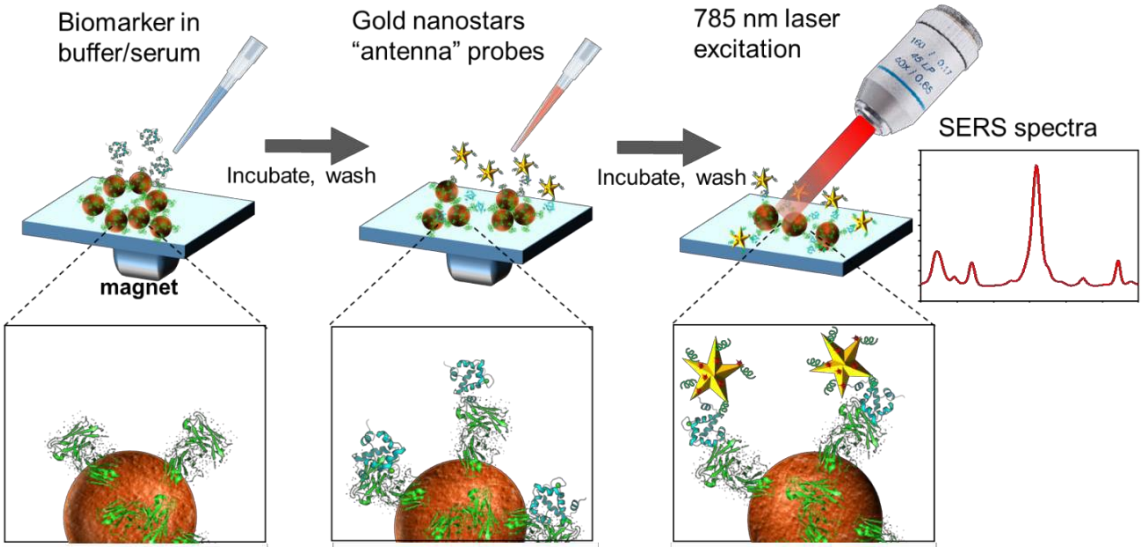

Figure 2.1. Schematic describing the principle of PRADA. Antibody-conjugated magnetic microbeads are incubated with the antigen in buffer or serum to capture the biomarkers. Raman reporter labeled GNS "antenna" detection probes, with peptide recognition elements, then form a sandwich immunocomplex, followed by magnetic separation and excitation with 785 nm laser to enable SERS based detection.

The sensitivity and specificity of PRADA is governed by the controlled synthesis of the capture and detection probes as shown in Figure 2.2. The composition of the resulting sandwich immunocomplex is directed by the specific interaction between the corresponding peptides, antigens, and antibodies. Here the capture probes are prepared by activating carboxylic acid-functionalized magnetic microbeads via EDC coupling (1-Ethyl-3-(3-dimethylaminopropyl)carbodiimide) and subsequent functionalization with anti-cTnI polyclonal Abs (or anti-NPY pAbs). The sandwich immunocomplex is completed with ~65 nm GNSs covalently conjugated with Raman reporter via Au-thiol bonds and small peptide biorecognition elements. cTnI detection was enabled with DTNB (5,5′-Dithiobis(2-nitrobenzoic acid)) reporters and P2 peptides, and NPY detection was facilitated with pMBA (para-mercaptobenzoic acid) reporter and NP3 peptide. The human troponin I binding peptide P2 (WQIAYNEHQWQ*GGGC*), computationally evolved from a phage display peptide has nanomolar binding affinity to cTnI.[74] The bioconjugation of the peptide to GNSs is achieved via Au-S linkage by introducing a cysteine

residue at the C-terminus of the peptide. A tri-glycine spacer domain is inserted between the C-terminal cysteine and the P2 peptide to extend the binding domain away from the gold surface. The NPY binding peptide NP3 (FPNWSLRPMNQM*GGGC*) was also identified from a phage display peptide library. These dodecapeptides have an average size of 2 - 3 nm which is significantly smaller than antibodies (~10 nm) allowing ultrasensitive detection of cTnI and NPY in both buffer and serum due to its closer proximity to the gold surface. DTNB and pMBA are ideal Raman reporters for this platform since (i) they are covalently bound to the gold surface, enabling both high stability and SERS signal amplification via electromagnetic and chemical enhancement, and (ii) their primary Raman peaks at 1325 cm^{-1} (DTNB) and 1580 cm^{-1} (pMBA) do not overlap, enabling multiplexed detection of both biomarkers.

The overall dimensions of the GNS detection probes are ~65 ± 7 nm (branch-to-branch length) which results in a plasmon resonance centered at 780 – 790 nm (Fig.2b). After functionalization with Raman molecules and peptides an overall ~13 nm redshift in plasmon resonance was noted due to an increase in hydrodynamic size and change in refractive index of the functionalized GNSs (Fig. 2.2c). The SERS footprint of the peptide and DTNB conjugated GNSs demonstrated a clear peak at 1325 cm^{-1} corresponding to the symmetric stretching mode of the nitro group of DTNB (Fig. 2.2d).[75] We demonstrated the ultrasensitive diagnostic capability of PRADA by monitoring the 1325 cm^{-1} peak of DTNB corresponding to cTnI concentration. The DTNB peak decreases with decreasing concentration of cTnI in the range of 0.03-1000 ng/mL (Fig. 2.3a). The SERS intensities enabled us to generate a sensitivity and specificity curve (Fig. 2.3b) allowing us to calculate the limit of detection (LOD) of cTnI. PRADA enabled a LOD of 0.03 ng/mL of cTnI which surpasses the LOD of commercial ELISA platforms at >0.1 ng/mL (Fig. 2.6). The clinical cTnI range for at-risk patients is 0.1 to 10 ng/mL but much lower (≤ 0.04 ng/mL)

concentrations are of interest for risk stratification. This high sensitivity of PRADA is attributed to the use of short peptides in this platform that bind to regions of the target cTnI without competing with the antibody, and the intense near-fields of nanostars that contributes to enhanced SERS signals.

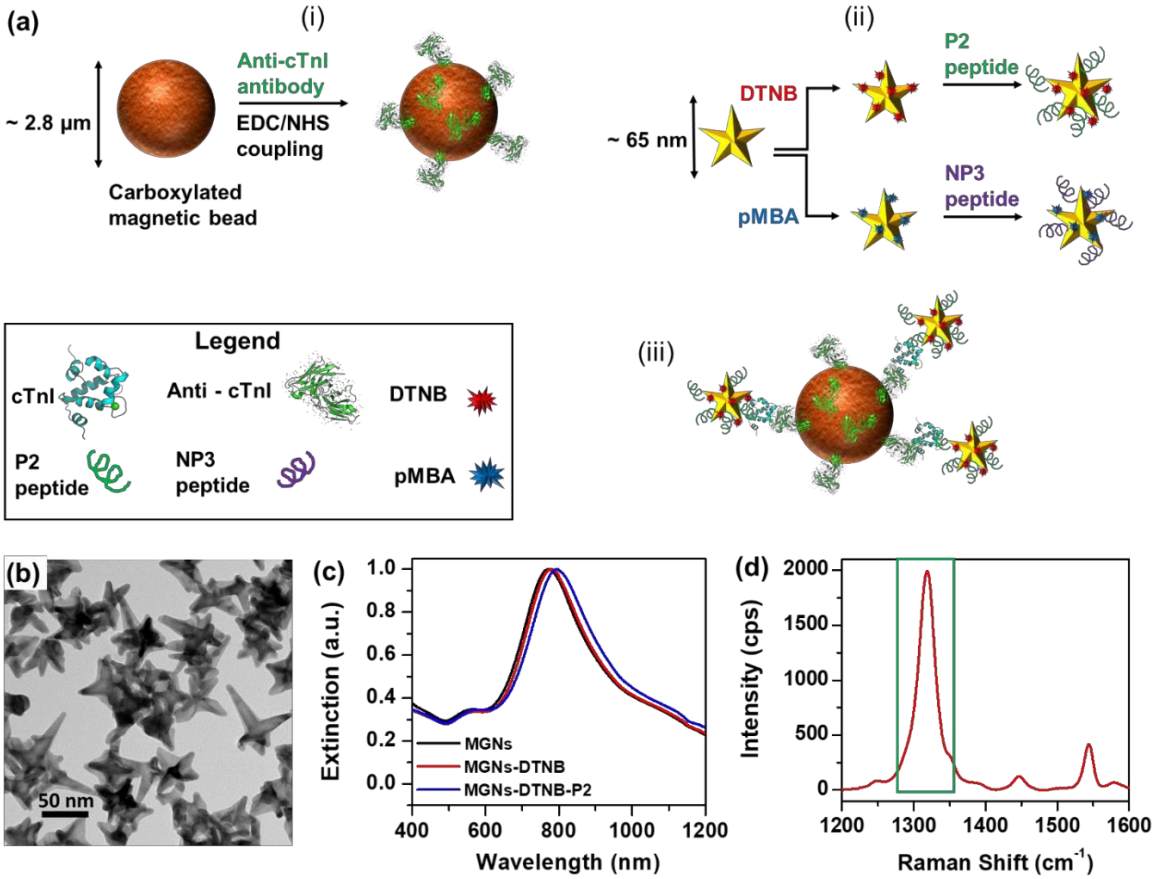

Figure 2.2. (a) Schematic representing synthesis of capture and detection probes. (i) Magnetic microbeads are functionalized with polyclonal antibodies (ii) GNSs are conjugated with Raman reporters and targeting. (iii) The complete PRADA immunocomplex formed by magnetic microbead capture probes, target antigen cardiac troponin I (cTnI), and nanostar detection probes. Characterization of detection probes. (b) TEM (Transmission Electron Microscopy) micrograph of GNSs. (c) Extinction spectra showing the red-shift in plasmon resonance of nanostars after functionalization with Raman tag DTNB, and P2 peptide. (d) Raman spectra of nanostars after functionalization. The green box indicates the signature peak of DTNB at 1325 cm^{-1}.

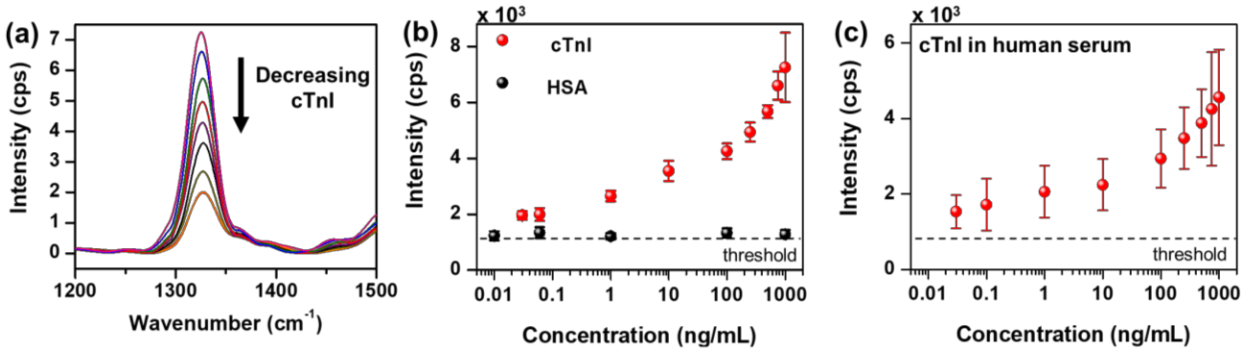

Figure 2.3 (a) Concentration-dependent SERS detection of cardiac troponin I (cTnI) in PBS buffer from 0 to 1000 ng/mL with a 785 nm laser by monitoring the DTNB peak, at 1325 cm^{-1}. (b) SERS intensity at the characteristic DTNB peak as a function of troponin and human serum albumin (HSA) concentration above noise threshold. (c) Intensity of Raman signal at characteristic DTNB peak as a function of troponin concentration in commercially obtained de-identified human serum showing a LOD of 0.03 ng/mL.

We also demonstrated the specificity of PRADA by examining different concentrations of human serum albumin (HSA) in the 0.01-1000 ng/mL range with anti-cTnI pAbs-coated capture probes and DTNB/P2 peptide-coated detection probes (Fig. 2.3b). The SERS intensities for HSA were at the noise threshold irrespective of concentration, confirming the high specificity of PRADA in accurately detecting ultralow concentrations of cTnI with minimal cross-reactivity with other competing proteins. Further, we evaluated the potential of PRADA for biomarker detection in clinical samples using commercially available deidentified human serum (Discovery Technologies) that was spiked with cTnI in the range of 0.01-1000 ng/mL (Fig. 2.3c). PRADA demonstrated an accurate LOD of 0.03 ng/mL in human serum consistent with that achieved in buffered solutions (Fig. 2.3c). The SERS intensity of DTNB increased with a rise in cTnI concentration in serum. Whereas the SERS signal is lower in serum than in buffer for comparative concentrations of cTnI, this is expected as unbound cTnI must compete with other serum constituents to be captured by the magnetic microbeads. Human serum contains approximately 4000 metabolites,[76, 77] which would compete to bind to the targeted site. Our results clearly

demonstrate that PRADA is a versatile platform for rapid and quantitative analysis of biomarkers of cardiac health in human biofluids with high sensitivity and specificity.

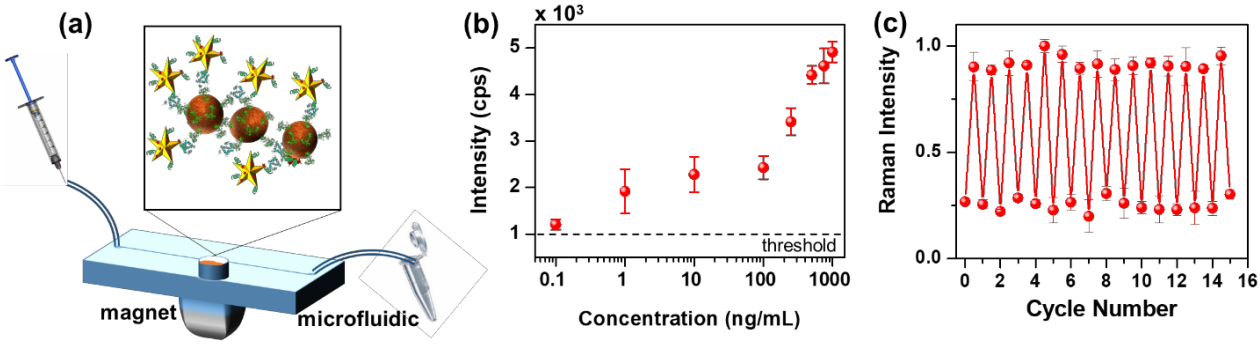

Figure 2.4 (a) Schematic showing the translation of PRADA to a single-well microfluidic device. (b) cTnI detection via SERS in single-well microfluidic showing a clinically-relevant detection limit of 0.1 ng/mL above noise threshold. (c) Demonstration of reusability of PRADA over 15 cycles where 100 ng/mL of cTnI was detected via SERS at the DTNB Raman peak with minimal signal loss. The first point of the reusability data contained no antigen and the devices were washed in between the cycles by removing the magnet, flushing out the used magnetic beads and replenishing the wells with freshly functionalized capture probes to perform a new assay.

We also translated PRADA to a microfluidic device to enable multiplexed biomarker detection in small sample volumes (~50 µL) with rapid washing and reusability of the same device over multiple cycles. A microfluidic device with a two-layer PDMS/glass assembly was developed with an immunoassay chamber connected to an inlet and an outlet (Fig. 2.4a).[78] PRADA was assembled in the microfluidic wells by first introducing the magnetic microbead capture probes, which were subsequently held in place with a magnet. This was followed by introducing cTnI at varying concentrations and, afterwards, the nanostar detection probes. After three washes to remove unbound biomarkers and detection probes, the resulting immunocomplexes were analyzed with SERS, demonstrating a clinically-relevant LOD of 0.1 ng/mL in the microfluidic devices. Next we demonstrated reusability by recycling the same microfluidic device to detect 100 ng/mL of cTnI over 15 cycles by repeated washing and reusing (Fig. 2.4c). The reusability of PRADA is enabled by the magnetic microbeads, as removal of the magnet allows us to wash off

the entire resulting complex formed with the capture probe, detection probe, and antigen, and regenerate the microfluidic sensor chip for multiple uses. Our regeneration approach has several merits – (i) PRADA has <4% signal loss after multiple cycles, which outperforms chemical regeneration approaches that have been reported to have 10–50% signal loss during each cycle.[79] In chemical regeneration, low pH glycine buffer or detergent solutions are introduced to detach the antigens from antibodies, enabling reusability of the sensor chip with the same set of antibodies between samples.[80] However chemical regeneration is ineffective when using patient biofluids due to the presence of bacteria, proteases, and other enzymes etc. that can rapidly degrade these antibodies.[81] This emphasizes the strength of PRADA and our magnetic regeneration approach. (ii) Prior to regeneration, the microbead/antigen/nanostar immunocomplex representing each sample can be archived (by removing the magnet) for future analysis. This is facilitated by the stability of the Raman tags, as they do not photobleach and are amenable to long-term storage. Therefore, our results suggest microfluidics-based PRADA will ultimately enable a low-cost platform that can be regenerated multiple times, allowing rapid and accurate assessment of multiple biomarkers from many patient samples.

Multiplexed detection enabling rapid and quantitative bioanalysis of multiple analytes in a single sample is of significant interest to predict the complex phenotype of many disorders. PRADA translated to a microfluidic device is ideal for multiplexing enabled by the narrow spectral features of SERS that offers high sensitivity and minimum overlap between corresponding Raman reporters. We simultaneously detected cTnI and NPY (Fig. 2.5) by using a 1:1 mixture of magnetic microbeads conjugated with anti-cTnI pAbs and anti-NPY pAbs respectively which served as the capture probes in the single-well microfluidic devices. After a brief washing step, buffer samples with no antigen (control), 250 ng/mL cTnI, 250 ng/mL NPY, or 1:1 mixture of 100 ng/mL cTnI +

100 ng/mL NPY were incubated with the capture probes. After removing unbound antigens with a rapid washing step, 1:1 mixture of detection probes targeting cTnI (P2-DTNB-nanostars) and NPY (NP3-pMBA-nanostars) were incubated. Multiplexed detection was successful with PRADA where clear peaks of DTNB (1325 cm^{-1}) and pMBA (1580 cm^{-1}) were observable with minimal non-specific binding for the no antigen control. We also note that each of these assays was performed after repeated washing and reusing the same microfluidic device. In addition to multiplexed biomarker detection, we also demonstrated multiplexed sample analysis to mimic the diagnosis of multiple patient samples simultaneously. This would be particularly relevant for field-use or in resource limited settings where several patient samples have to be rapidly analyzed to determine the status of their cardiac health (cTnI) and fatigue/stress (NPY). Here we designed a 3-well microfluidic device for multiplexed sample analysis and introduced a mixture of the two capture probes as described above. We then spiked commercially available human serum (Discovery technologies) with different amounts of cTnI and NPY to mimic patient samples with varying degrees of cardiac dysfunction and anxiety. We interrogated three different model patient samples including low levels of cTnI (0.05 ng/mL) and NPY (0.05 ng/mL), elevated NPY (0.45 ng/mL + 0.05 ng/mL cTnI), and elevated cTnI (0.45 ng/mL + 0.05 ng/mL NPY). The SERS spectral peaks observed in the 3-well microfluidic device is in accordance with the trend observed in the single-well device (Fig. 2.5b) where an increase in DTNB (1325 cm^{-1}) or pMBA (1580 cm^{-1}) signal corresponds to elevated cTnI and NPY respectively. The background Raman signal between 1350–1500 cm^{-1} is from the proteins in the serum. Note: DTNB has another characteristic peak at 1550 cm^{-1} which appears as a shoulder in the elevated cTnI spectrum. These results demonstrate PRADA is a robust multiuse platform that allow diagnosis of multiple biomarkers of

interest within minutes and has the potential to analyze patient samples in biofluids with high accuracy and specificity.

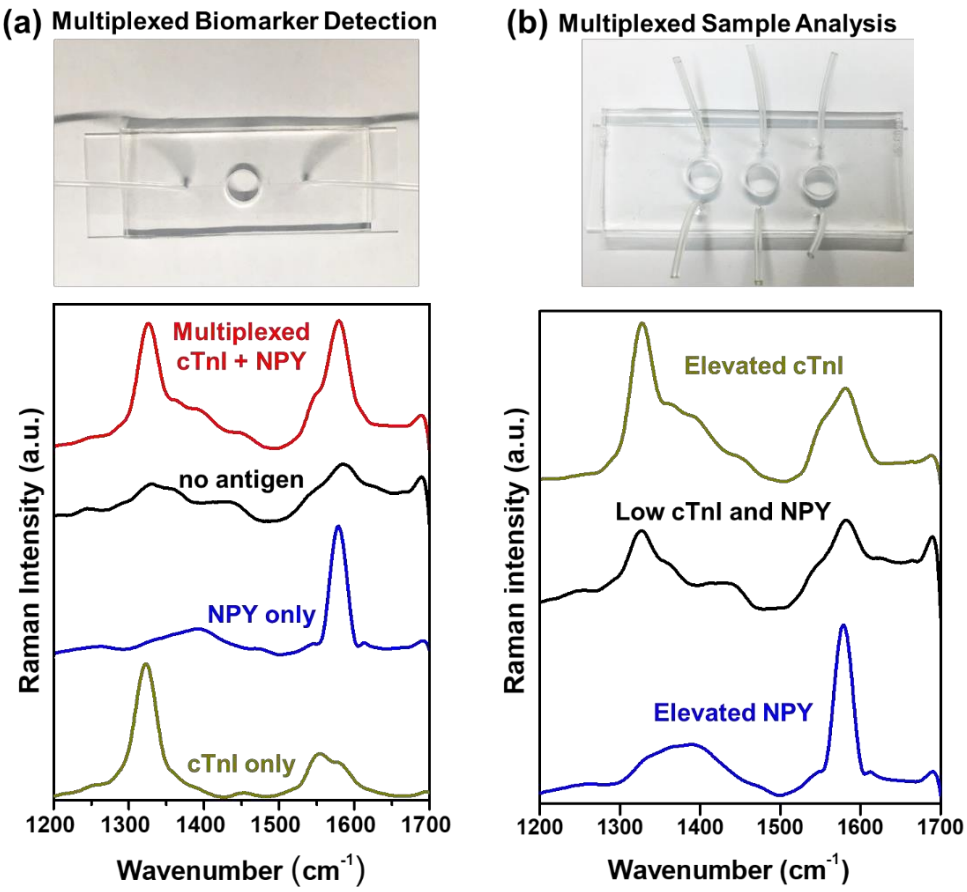

Figure 2.5 Multiplexed detection of both cardiac troponin I (cTnI) and neuropeptide Y (NPY). (a) Multiplexed detection of both biomarkers in a single-well microfluidic device. The same microfluidic was washed and reused for the single biomarker and no antigen assay showing both specificity and reusability. (b) Simultaneous multiplexed biomarker detection and multiplexed "patient" sample analysis in a 3-well microfluidic device. Here patient samples are mimicked by spiking commercial de-identified human serum with various concentrations of cTnI and NPY. This includes low levels of cTnI (0.05 ng/mL) and NPY (0.05 ng/mL), elevated NPY (0.45 ng/mL + 0.05 ng/mL cTnI) and elevated cTnI (0.45 ng/mL + 0.05 ng/mL NPY).

2.4 Conclusions

In summary, this study presents an innovative sandwich immunoassay platform, PRADA, where magnetic microbeads capture biomarkers from serum or buffer samples and GNS

“antennas” diagnose the biomarkers using SERS-based detection. We have shown ultrasensitive PRADA detect cTnI, a biomarker of myocardial infarction, with a LOD of 30 pg/mL in both buffered samples and in commercially available human serum superseding the LOD of 125 pg/mL of standard ELISA for cTnI (Figure 2.6). Further, by translating PRADA to a simple microfluidic device, we demonstrated multiplexed detection of cTnI and NPY, a biomarker of fatigue and stress, with high specificity and sensitivity in low sample samples. We also showed PRADA is a reusable platform enabling regeneration and multiple uses of the same microfluidic chip with <4% signal loss between cycles, and allowing to archive samples for future bioanalysis. Our results show PRADA may ultimately enable a high throughput point-of-care diagnostic with rapid, and early prediction of patients with acute coronary syndromes or chronic fatigue syndrome,[82-84] enabling accurate assessment of risk status. Further the rapid readout time (10 minutes per sample) with SERS, regeneration and reusability, and use of small sample volumes will ultimately enable PRADA’s utility in resource-limited settings where a low-cost and user-friendly point-of-care is necessary for rapid analysis of patient samples. Whereas in this proof-of-concept study we demonstrate multiplexing of two biomarkers in human serum, our future work focuses on the use of clinical patient samples where PRADA will allow the detection of >10 biomarkers enabled by the narrow spectral features of SERS and reusability over 100 cycles to translate PRADA from bench to bedside. We envision that PRADA will ultimately enable a precise scoring system to determine patient outcome which can be ultimately integrated with smart phones for cost-effective health monitoring.[79, 85]

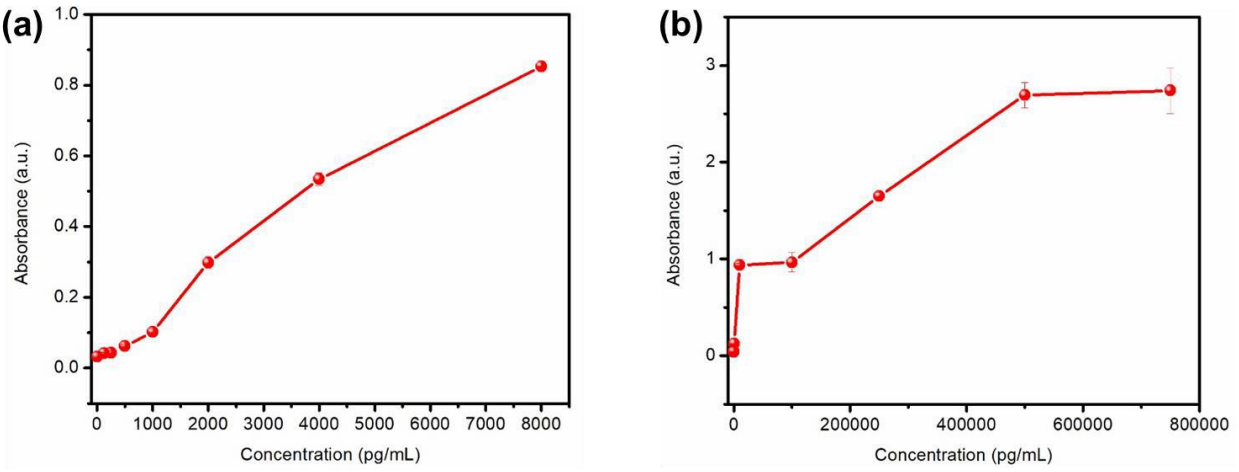

Figure 2.6 (a) Standard curve from ELISA kit (Invitrogen) for human cTnI. (b) cTnI detection from buffer samples using ELISA kit. The lowest concentration of cTnI measured with ELISA when compared to the standard curve at an absorbance of 0.04 is at 125 pg/mL, which is in accordance with the manufacturer's detection limit at >100 pg/mL.

Limitations of approaches used in this work

PRADA is a highly sensitive platform and the sensitivities attained with PRADA can drastically differ when the conditions of assay development are optimized for the best conditions. There were several conditions of PRADA that could be optimized and improved to achieve higher limit of detection, and higher reproducibility of the results presented here.

The glass slides and microfluidic devices should be passivated with a PEG silane linker and Tween 20 to minimize background noise and non-specific binding. This is a crucial step and in the results presented in this thesis, this step was either missed or improperly conducted which often resulted in high background and low signal to noise in Raman signal. This is reflected in the inconsistency in SERS intensity observed when PRADA was performed on plain glass vs in microfluidic channels. The microfluidics uses the same microscope glass so SERS signal should not have been so different.

Prior to conjugation of polyclonal antibodies to the magnetic microbeads, EDC coupling was performed to activate the carboxylate groups with NHS ester. This reaction should be

executed in 25 mM MES buffer at basic pH, however I performed this in PBS buffer. The EDC coupling reaction is significantly less efficient and often does not complete in PBS buffer. MES buffer is recommended instead.

After the EDC coupling reaction culminates, the microbeads should be incubated in Tris buffer at pH 7.4 to quench all unreacted carboxylic acids. This step was not performed in the results presented here and should be executed in future work.

The troponin/NPY proteins (or antigens) stock solution should have been aliquoted and redispersed in TBS buffer. Instead the proteins were aliquoted in water and stored at -20 C. This would have resulted in freezing and ultimately denaturing of the proteins before PRADA was performed for antigen detection. Therefore the results presented here can significantly vary and can likely be improved when the proteins are handled in TBS buffer.

There were multiple reactions such as conjugation of peptides to nanostars, conjugation of antibodies to microbeads etc. were performed overnight. But these reaction times can be shortened to a few hours to minimize aggregation of nano/micro particles and improving the detection limits of PRADA.

Background subtraction in Raman is essential to remove noise from the substrate or any undesirable fluorescence from the reagents used. This is a crucial step to determine the correct limit of detection. I ran into challenges in the multiplexing assay with cTnI and NPY and as such background subtraction was not performed correctly. With proper background subtraction, the multiplexed detection results could be easily quantified to determine when a patient could be categorized as high risk or low risk.

2.5 Experimental Methods

Synthesis and functionalization of magnetic microbeads capture probes

For conjugation of cTnI antibodies on the surface of magnetic beads, 50 µL of 50 mg/mL EDC and 50 µL of 50 mg/mL NHS were added to 10 µL of Dynabeads M-270 Carboxylic Acid magnetic beads (Life Technologies, cat. no. 14305D) and allowed to react for 30 min with gentle mixing at room temperature. After incubation, the beads were separated by magnet and washed twice with 1X PBS buffer solution. The beads were resuspended in 995 µL 1X PBS buffer solution and reacted with 5 µL of 0.2 mg/mL rabbit polyclonal cardiac Troponin I antibody (Abcam, cat. no. ab47003)/5 µL of 0.2 mg/mL rabbit polyclonal neuropeptide Y antibody (Abcam, cat. no. ab30914)/ 40 µL of 0.2 mg/mL normal mouse IgG (Santa Cruz Biotechnology, cat. no. sc-2025) for 8 h with gentle mixing at 4 °C. Unreacted antibodies were removed by washing the beads three times with 1X PBS buffer. The unreacted –COOH groups were deactivated following the addition of 100 µL of 50 mM Tris buffer solution and incubation for 1 h at 4 °C. After washing the beads twice with 1X PBS buffer solution, the final product was stored in 100 µL of 1X PBS at 4 °C for future use.

Synthesis and characterization of GNS detection probes

GNSs were synthesized by following our previously described procedure that utilizes a one-step seedless growth mechanism. In this process, the gold precursor Au^{3+} is reduced and capped by HEPES (4-(2-Hydroxyethyl)piperazine-1-ethanesulfonic acid, N-(2-Hydroxyethyl)piperazine-N′-(2-ethanesulfonic acid)) (Sigma Aldrich, cat. No. H3375), a biological buffer. The adsorption of HEPES along the <111> plane allows for kinetically driven protrusion growth in the same direction, whereby the core-to-protrusion ratio is controlled by the concentration of HEPES used in the synthesis. First, 1 mL of 20 mM $HAuCl_4$ was prepared by

diluting the stock solution. Then, 24 mL of 180 mM HEPES was mixed gently with 36 mL of ultrapure water (18.2 MΩ obtained from a Milli-Q Direct-Q 3UV system). Later, 600 µL of 20 mM $HauCl_4$ was then mixed in at room temperature and allowed to mix gently for 2 min before letting the solution stand for 1.25 h. At this stage the color of the gold colloids changed to greyish-black, indicating the formation of the GNSs. By using 180 mM HEPES, we tuned the plasmon resonance of the GNSs to roughly 785 nm. Two different types of SERS nano-tags were prepared for the simultaneous detection of cTnI and neuropeptide Y. First, two Raman reporters, 3 µL of 10 mM DTNB (5,5′-Dithiobis(2-nitrobenzoic acid) (TCI America, cat. no. D0944) and 3 µL of 10 mM pMBA (para-mercaptobenzoic acid) (TCI America, cat. no. M1294), both prepared in cold 100% ethanol, were added to each 30 mL of the GNS solution respectively. After gentle mixing at 4 °C for 15 min and 10 min respectively, the shift in plasmon resonance was measured due to the binding event via thiol linkage. The GNSs were then purified through three rounds of centrifugation (6000 rpm, 20 min) and each batch redispersed in 1 mL MilliQ water. The DTNB-conjugated GNSs were mixed with 20 µL of 1 mg/mL P2 peptide (-WQIAYNEHQWQGGGC-) (Genscript), and the pMBA-conjugated GNSs were mixed with 20 µL of 1 mg/mL NP3 peptide (-FPNWSLRPMNQMGGGC-) (Genscript) gently overnight at 4 °C. Excess peptides were removed through one round of centrifugation (6000 rpm, 20 min) and resuspended in 1 mL MilliQ water. Peptide coating was then checked by measuring the shift in plasmon resonance.

Biomarker capture and SERS detection in serum and buffer

To assess the diagnostic capacity and the clinical applicability of the proposed immunoassay, we performed the assays on clinical research serum samples (Discovery Life Sciences, cat. no. DLS15-14811) that were spiked with different concentrations of cTnI antigen varying between 0.01 and 1000 ng/mL. This study was approved by the Institutional Review Board

(IRB) at Vanderbilt University. All serum samples were stored at -80 °C until use. The prepared antibody-coated magnetic beads were split into nine Eppendorf tubes into which 100 µL of the desired concentration-spiked serum is added, and allowed to mix for 8 h at 4 °C. Unbound antigen was then removed from the samples by washing three times with 1X PBS. The nine samples were then each suspended in 100 µL of DTNB-conjugated GNSs and allowed to mix gently overnight at 4 °C. The resulting immunocomplexes were then separated using a magnet and washed thrice with MilliQ water before drying on separate passivated glass slides for 5 h and then imaged using an inVia Raman microscope (Renishaw).

The immunoassay was repeated with similar steps but substituting serum with 1X PBS buffer solution. As a negative control, a separate batch of antibody beads were prepared and split into five Eppendorf tubes and allowed to mix with 100 µL each of 0.01, 0.06, 1, 100, and 1000 ng/mL of human serum albumin (HSA) (Sigma Aldrich, cat. no. A5843) for 8 h at 4 °C. After washing off unbound HSA three times with 1X PBS, the samples were then suspended in 100 µL of DTNB-conjugated GNSs and allowed to mix overnight at 4 °C. The samples were subsequently washed three times with MilliQ water before drying on passivated glass slide in preparation for Raman imaging.

Microfluidic device fabrication

All steps regarding the fabrication of various microchannel patterns was performed using facilities within the cleanroom affiliated with the Vanderbilt Institute of Nanoscale Science and Engineering (VINSE). To make a microchannel mold, mr-DWL_40 resist was cast on a clean silicon wafer and spin-coated at 1000 rpm for 60s, yielding a 60 µm-thick resist layer. Then, designed patterns was directly written into the photoresist using a laser writer (Heidelberg µPG 101). The wafer with patterned resist was coated with a thin layer of silane to facilitate subsequent

removal. To make a microfluidic device, liquid polydimethylsiloxane (PDMS) (Sylgard 184) was mixed in a 1:10 ratio of curing agent and PDMS resin, degassed in a desiccator and carefully poured onto the resist mold placed in a petri dish. After curing in an oven at 65 ℃ for 12 h, the PDMS layer was cut and peeled off the resist mold. Holes were punched at the inlet and outlet of the microchannels using a 8.5 mm internal diameter punch (Ted Pella, cat. no. 15084). A clean microscope glass slide (Fisher Scientific, Premium Plain Glass Microscope Slides, cat. no. 125444) was bonded to the patterned PDMS layer by exposing to an oxygen plasma (Harrick Plasma, PDC-001) for 60 seconds. The resulting device was baked on a hot plate at 60 ℃ for 1 h before use.

Multiplexed biomarker detection in microfluidic devices

In order to assess the reusability and feasibility in multiplexing of the microfluidic device, 50 µL of anti-cTnI beads, IgG beads, and anti-NPY beads were flowed through each outlet channel and collected in the well, aided by the magnet secured in the chip-holder. After washing the channels three times with 1X PBS buffer solution, flowed in through the inlet channel, 50 µL 250 ng/mL cTnI and/or NPY was flowed through the inlet channel and allowed to mix on an orbital shaker at 4 °C for 8 h. 1X PBS buffer was used to wash the beads through the inlet channel, and then collected by suctioning the waste PBS with a syringe from the outlet channel. 50 µL of DTNB-conjugated GNSs and/or pMBA-conjugated GNSs were flowed through the inlet channel and pooled in the well and allowed to mix on an orbital shaker at 4 °C for 8 h. The unbound GNSs were suctioned out by a syringe as waste, and the well was washed three times with Milli-Q water, before being left to dry for 5 h and later imaged by the inVia Raman microscope.

ELISA

The cTnI antigens used for the ELISA were identical to the ones used for the proposed platform. Buffer samples and controls were prediluted according to the manufacturer's protocol without any adaptation (Invitrogen, cat. no. EHTNNI3). For the reference, a 2-fold serial dilution over 8 wells was tested. For each buffer sample, the same concentrations tested for SERS detection in buffer were used. Quantification of the antibodies against cTnI was then performed according to the manufacturer's protocol. A standard curve was generated for the reference by plotting the average absorbance (450 nm minus 550 nm) obtained for each of the standard concentration on the Y-axis vs. the corresponding cTnI concentration on the X-axis. The same was done for the buffer samples.

CHAPTER 3

LIPOSOME-GOLD HYBRID NANOSTRUCTURES, A NOVEL APPROACH TO COMBINED PHOTOTHERMAL CHEMOTHERAPY

3.1 Summary

Plasmon resonant gold nanoparticles of different sizes have been studied for their many applications in drug delivery, imaging, and photothermal therapy. Unfortunately, their capacity to degrade under physiological conditions after performing their function is limiting.[86] When used in combination with biodegradable liposomes, the gold nanostructures' capacity to degrade improves. The ~100-120 nm sized liposome-gold constructs break down to form smaller ~5 nm sized particles that successfully achieve renal clearance.[87] DPPC (1,2-dipalmitoyl-sn-glycero-3-phosphocholine): MSPC (1-stearoyl-2-hydroxy-sn-glycero-3-phosphocholine):PEG-2000 (1,2- distearoyl-sn-glycero-3-phosphoethanolamine-N-[amino(polyethylene glycol)-2000]) (90:10:4, molar ratio) liposomes are synthesized and remotely loaded with Doxorubicin, a chemotherapeutic agent, and coated with gold by *in situ* reduction of chloroauric acid using ascorbic acid as a reducing agent. The resulting nanoparticles, or plasmonsomes (from *plasmo*nic lipo*somes*), have been analyzed for their resonances and their photothermal capacities, as the liposome-gold constructs are produced within the "water window" range in which human tissue absorbs the least amount of light allowing for maximum physiological transparency and thus excellent radiation penetration for photothermal therapy.

3.2 Introduction

Gold nanoparticles have been extensively researched for their efficiency in photothermal therapy, and structured or shape variations such as nanoshells, nanorods, and nanocages have been

explored for their applications in the treatment of cancer.[88] While gold is biocompatible, it is not biodegradable – a disadvantage in that the prolonged retention of the nanoparticles is obstructive to diagnosis and prognosis.[89] Inorganic particles with a diameter smaller than 5 nm can be cleared through the renal system; however, nanoparticles useful for studies of photothermal therapy (PTT) are typically larger than 20 nm and are unable to be cleared by the renal system. Their accumulation in the reticulo-endothelial system (liver, spleen, and kidneys) has also proven toxic.[90]

Leung et al. developed a system that combines the properties of a phospholipid bilayer liposome and gold for drug delivery purposes.[91] Liposomes of certain compositions have been shown to be capable of thermally controlled release of encapsulated agents.[92] The thermal release of the inner contents of the liposomes occurs at specific temperatures that correspond to phase transitions. The current issue faced in clinical application is that the local temperature modulation necessary for spatial and temporal control of release is fairly difficult to achieve. The light-controlled content release will allow for precise and on-demand content delivery within individual cells *in vitro* or, when used in conjunction with endoscopic light delivery, can be used for precise medical intervention *in vivo*.[92] By coating the outer surface of a dipalmitoyl phosphatidyl choline (DPPC) liposome, they produced a core-shell effect to provide an absorbance in the near infra-red region that would be suitable for photothermal mediated drug release.[93] The use of near infra-red light promotes a greater depth of penetration with reduced damage to tissue. The benefit of using DPPC in the lipid core is that it is biodegradable.[94] Further after reaching its phase transition temperature, the DPPC liposome destabilizes and can release encapsulated drug/substance. As the phase transition temperature of DPPC is 41 ºC, it can encapsulate a drug and release it above body temperature.[95] Since cancer cells respond to temperatures above 43 ºC for thermal killing, it is necessary to achieve a composition that would enable drug release at this

temperature.[96] Further as the lipid bilayer degrades to release the drug, the gold nanoparticles that coat the surface split into structures small enough to be cleared through the renal system.

Among treatment modalities for cancer, chemotherapy is particularly disappointing since it contributes roughly 2% to 5-year survival in all types of cancers.[97] While some yield lasting remission periods in certain cancers like acute lymphocytic leukemia and gestational choriocarcinoma, the utilization of most chemotherapeutic agents by their narrow therapeutic window.[98] New formulations such as Doxil, doxorubicin that is encapsulated in thermosensitive liposomes, have been designed to limit the systemic exposure to such drugs.[99] The reduction of cardiotoxicity that is often associated with doxorubicin use is an advantage of drug encapsulation within the liposome.[100] Also, this delivery system allows for a more efficient and successful accumulation of the drug at the tumor site, due to the enhanced permeability and retention (EPR) effect, that is made possible by the leaky vasculature and decreased lymphatic drainage that is typical of the tumor environment.[101] Further improvement of the efficacy can be achieved by targeted delivery.[102] To follow through with the proposition of executing controlled release, the substance,

i.e. the drug/molecule, encapsulated is released or activated on demand.[103] The most common and practical methods of activation can include local environmental stimuli such as local change of pH, or external stimuli like hyperthermia, or illumination with near infrared light (NIR).[104] The increase in temperature that causes the degradation of the liposomes indirectly kills the cancer cells, thus showing that the engineered liposome-gold constructs serve a dual purpose in delivering drugs to the site of interest as well as killing the cells by providing heat. Pradhan et al. used a lipid combination of 1,2-distearoyl-sn-glycero-3-phosphocholine : cholesterol (DSPC : CHOL) to

create liposomes for magnetic targeting and drug release with a phase transition temperature of 43 ºC.[105] The use of ascorbic acid as a reducing agent to deposit gold on the surface of liposomes for PTT of cancer has been explored.[88] In this paper, we designed a new gold-coated thermal-sensitive liposome (the low temperature sensitive liposome (LTSL)), composed of three lipids: DPPC; MSPC; and, PEG-2000, in a molar ratio of 90:10:4; DOX is also remotely loaded into these liposomes using a transmembrane pH gradient that is created when synthesizing them in buffer.[106] The preparations were characterized by electron microscopy techniques to confirm the formation of the gold coating on the surface of the liposomes.[104] The nanostructures have the potential to encapsulate therapeutic small molecules in the hydrophobic layer, thus serving as a vehicle for additional drug delivery in addition to photothermal therapy. We studied the tunability of these gold-coated liposomes, as well as their capacity for photothermal therapy and drug release during heating to obtain stable nanostructures that can be potentially used for light-activated hyperthermia drug delivery.

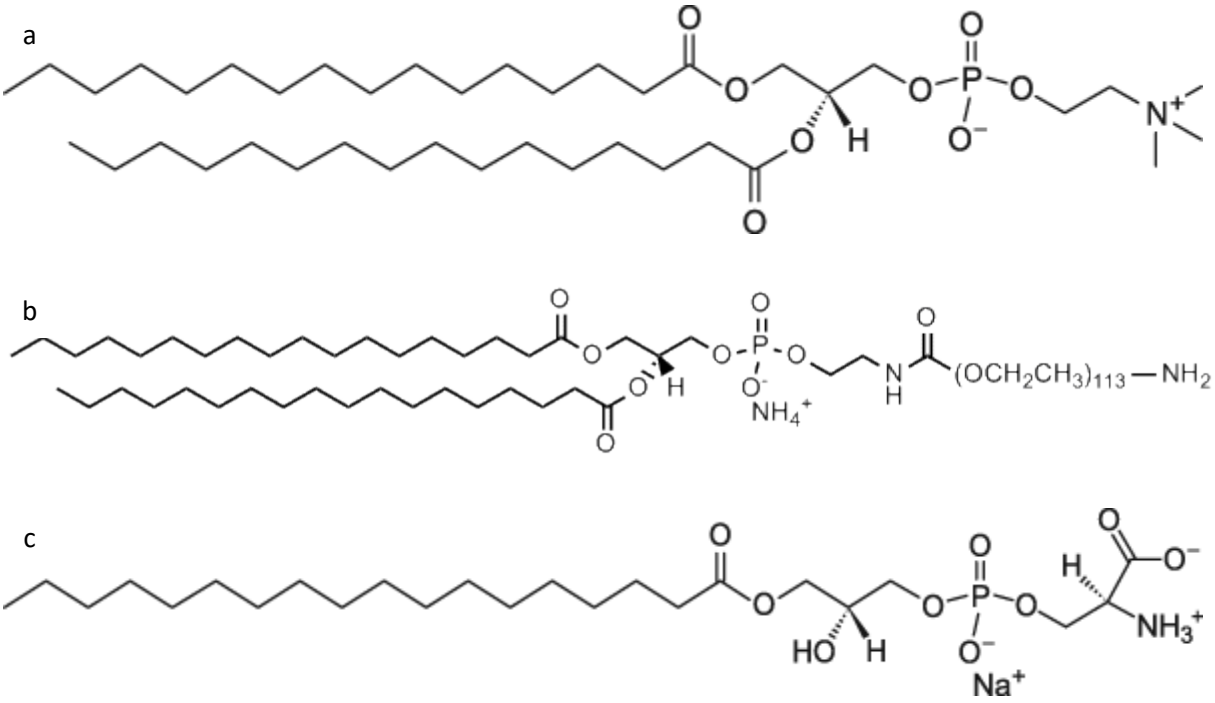

Figure 3.1 Chemical structures of (a) DPPC (b) DSPE-PEG2000, and (c) MSPC.

3.3 Results and Discussion

The DPPC : MSPC : PEG were prepared by thin film hydration method followed by coating the gold (in the presence of ascorbic acid (AA), which serves as a reducing agent to the chloroauric acid). The liposome-gold coating was optimized to contain 400 µg/mL lipid concentration, 20 mM of ascorbic acid and 6 mM of chloroauric acid, as observed in Figure 3.2. The reduction of gold on the surface of the liposome by using ascorbic acid as the reducing agent is given by the equation below (Figure 3.3). By varying the concentration of Au in the solution, we can tune the plasmonic properties of the particles to obtain the desired functions, i.e. be clinically relevant and applicable to the human system. It is observed that an increase in Au concentration results in a red-shift in plasmon resonance of the resulting particle.

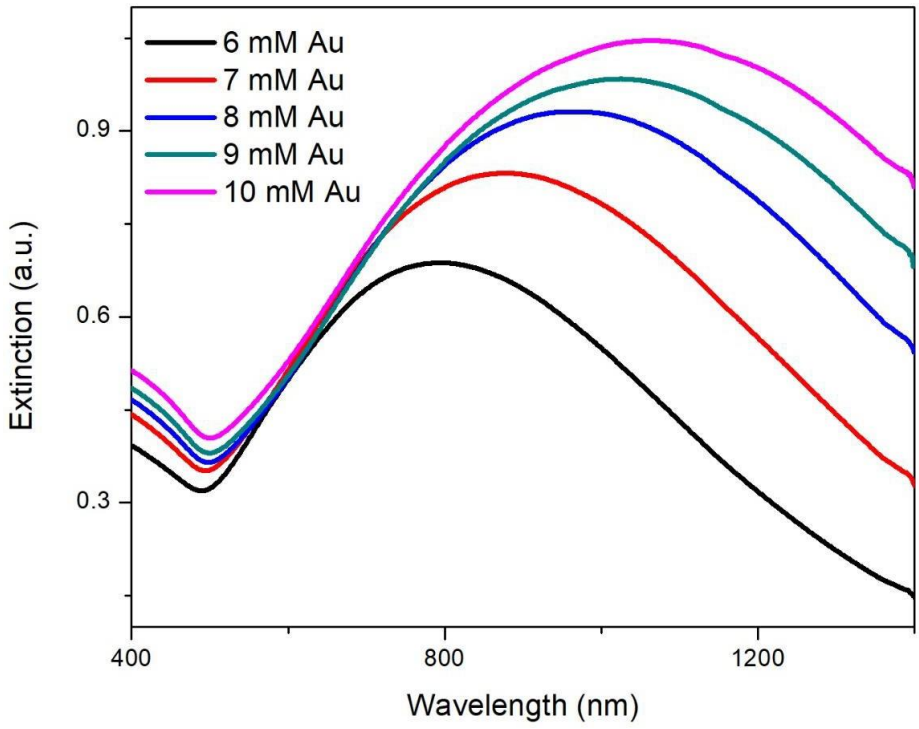

Figure 3.2 The changes in absorption and resonance due to the change in concentration of chloroauric acid; the higher the concentration of chloroauric acid, the greater the red-shift, making

them more tuned towards the “water window”.

The plasmon resonance frequency changes with the dimension because the electron oscillation has to accommodate the difference in the electromagnetic phase between one end of the particle, and the other.[107] The amplitude of the wave increases with the size of the particle, which in turn increases the period of each oscillation which is also referred to as the plasmonic lifetime.[21] An increase in the plasmonic lifetime results in the decrease in the frequency of the wave, means an increase in the wavelength and hence a red-shift in plasmon resonance, suggesting that there is an increase in the size of the particles.[108] The trend of increasing the concentration of gold in the formulation, that results in subsequent red-shifting of the nanoparticles, and hence increasing the size, is confirmed using TEM.

Step 1: Reduction of Au^{3+} to Au^{1+}

$$AuCl_4^- + 2e^- \longrightarrow AuCl_2^- + 2Cl^-$$

$$C_6H_8O_6 \longrightarrow C_6H_6O_6 + 2H^+ + 2e^-$$

Step 2: Reduction of Au^{1+} to Au^0

$$AuCl_2^- + e^- \longrightarrow Au + 2Cl^-$$

Overall Reaction of Au^{3+} to Au^0

$$2AuCl_4^- + 6e^- + 3C_6H_8O_6 \longrightarrow 2Au + 8Cl^- + 3C_6H_6O_6 + 6H^+$$

Figure 3.3: Chloroauric acid reduced by ascorbic acid to form gold coatings on the surface of liposomes.

The aforementioned composition for the LipoAu constructs was chosen since the resonance that was obtained was closest to the water window range (700 nm to 1100 nm).

We show in Figure 3.4a that the size of these particles was found to be 180 nm. TEM images as observed in Figure 3.4b show that the liposomes that were obtained indicated the size to be around 100-150 nm. We also performed DLS measurements on bare liposomes and found that the sizes are comparable both before and after gold coating, indicating the compact self-

assembly of gold on the liposome surface. Figure 3.4a also shows that the liposome-gold complexes were stable as individual particles and retained their multiple-protrusion morphology that owes to their resonance tuned to the IR region.

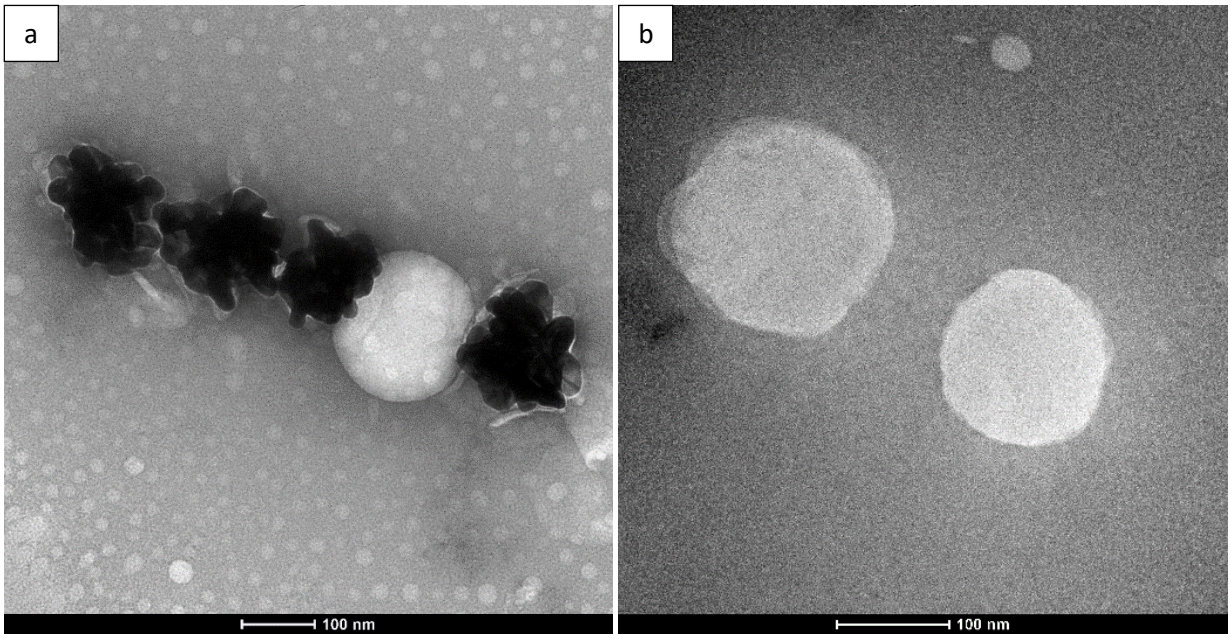

Figure 3.4. (a) TEM image of LipoAu synthesized using ascorbic acid, and bare liposome (second entity from right), **(b)** TEM image of bare liposome with methylamine tungstate as negative stain.

To show that the plasmon resonant liposomes were responsive to laser illumination, the samples were irradiated at 5 W/cm^2 power density with 808 nm continuous wavelength laser diode. Figure 3.5 shows that under laser illumination, 80 µg gold-coated liposomes/mL (the immediate resulting formulation of gold-coated liposomes), have the temperature increased to 47 °C from 23 ºC within the first 5 minutes. A greater temperature elevation was accomplished by increasing the concentration of gold-coated liposomes. 47 °C would be classified as mild hyperthermia and thus a high enough temperature for the release of encapsulated drug. This demonstrates that the gold-coated liposomes ability to convert light to heat is highly dependent on the concentration of the particles; the higher the concentration, the higher the temperature achieved after irradiating the

nanoparticles with the corresponding laser light.

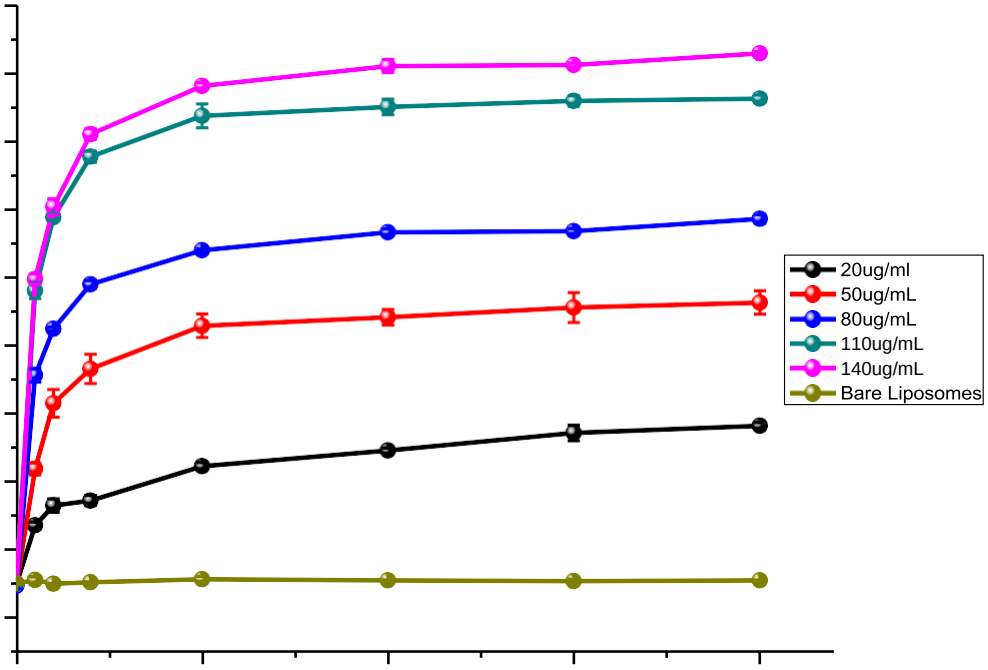

Figure 3.5 Varying the concentration of the gold-coated liposomes in solution and illuminating with a 808 nm laser shows the change in temperature; and increase in concentration corresponds to an increase in temperature of solution.

Doxorubicin-loading through the transmembrane sodium citrate (pH) gradient achieved 95-98 % encapsulation efficiency. High loading efficiency minimizes the use of expensive chemotherapy drug and prevents excess unloaded drug from entering the bloodstream; free doxorubicin is toxic to the system and this encapsulation thus allows for appropriate and less harmful biodistribution.[109] At body temperature, minimal doxorubicin was leaked out of the nanostructures over 20 minutes, as seen in Figure 3.6. Low leakage rate implies that light-activated drug release system can reduce doxorubicin's cardiotoxicity. On the other hand, at a temperature of 45 ºC, over 90% of doxorubicin was released in a period of 10 minutes. Moreover, since drugs will be released from these gold-coated liposomes at the tumor microenvironment, doxorubicin

can easily diffuse through the cellular membranes, thus eliminating the need of active cellular uptake.[110]

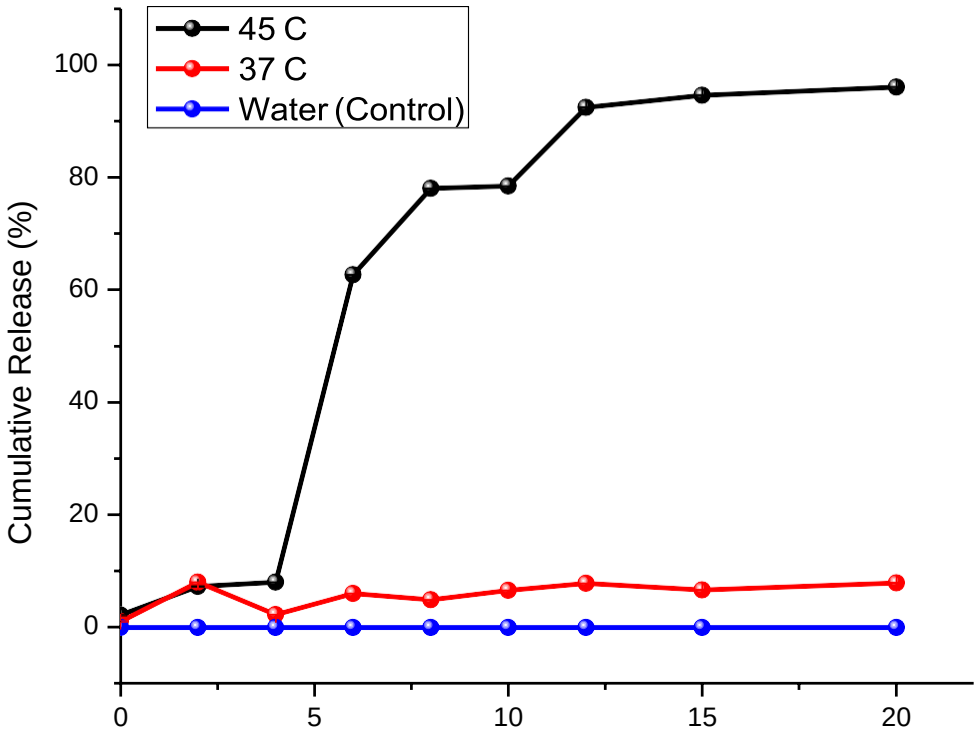

Figure 3.6 Changes in temperature results in varying degrees of DOX release. A temperature of 45°C, which is above the phase transition temperature allows for a cumulative release close to 100% after 10 minutes of exposure to heat.

However, upon examining the effects of NIR light on particle size post-illumination, it is observed that the disintegration of the gold-coating is not observed at all. The integrity of the structures remains unchanged, and the morphology does not look any different from that of the particles' pre-illumination (Figure 3.7).

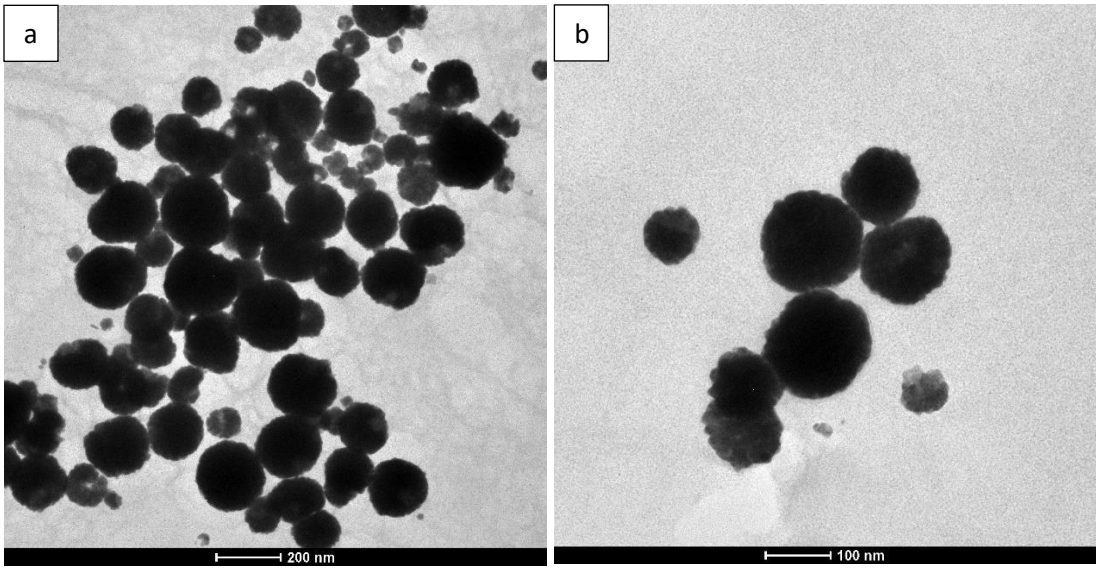

Figure 3.7. (a) TEM image of gold-coated liposome before PTT **(b)** TEM of a gold-coated liposome after PTT.

Looking further into existing literature, regarding trends in plasmon resonance changes for core-shell structures like the ones designed in this project, it is noted that the observation made with this formulation is consistent only with the theory for solid, "sphere-like" particles.[107]

The plasmon resonance of such shells is related to the interaction between the plasmons supported on the inner and outer surface of the gold shell. The strength of their interaction is determined by the shell thickness scaled by particle size.[111] As the gold shell decreases in thickness, a stronger plasmon interaction red shifts the resonant peak compared to that of a solid gold particle.[111] Theoretically, in the first round of direct adsorption of 1-2 nm small gold seeds, there will be only partial surface coverage that could be systematically improved by seeded reduction of additional gold salt onto the surface of liposomes.[112] Starting with the bare liposome, with increasing gold coverage, the plasmon resonance red-shifts from that of the smaller isolated gold nanoparticles that cluster on the surface, until the shell is complete.[113] Once the gold shell on the surface of the liposome is complete, the plasmon resonance blue-shifts with increasing shell thickness.[113] This particular phenomenon, as shown by Shi et al. in the case of gold shells on

silica cores, is understood in the framework of Mie scattering theory as increasing the multipole contributions to the extinction becomes significant with increasing shell thickness.[112] Thus, it is possible to conclude that the gold-liposome structures resulting from the above formulation were (a) solid gold nanoparticles that had seeded and grown inside the core of the thermally-sensitive liposome, or (b) incomplete gold shells on the surface of liposomes, even with the highest concentration of gold used in the formulation. The characterization of the particles using TEM did not yield discernable and distinct structures; liposomes are essentially not electron dense, and as such require negative staining in order to be observed under the microscope. The stain methylamine tungstate was used in an attempt to distinguish the liposomes from gold within the structure, but the results were not as clear to establish a concrete conclusion.[114] Cryo-TEM would have allowed the observation of the particles in their native solution, without having them come in contact with any other adhering surface, which would otherwise result in an altering of the shape of the structure.[115] Another advantage of cryo-TEM s that stains are not necessary, and so the specimen will not be distorted through the use of such dyes; also, using cryo-TEM will also enable the user to distinguish between lipids, which would be helpful in differentiating between parts of the particle that may be covered with gold and parts of the bare liposomes' surface.[116]

Upon further investigation into the formulation used to synthesize the gold-coated liposomes, it was noted that the lipid composition of DPPC, MSPC, and PEG-2000 yielded a negatively charged liposome;[117] this was confirmed by measuring the zeta potential of the liposomes. The gold particles that are reduced on the surface of the liposomes also had their zeta potential measured (Figure 3.8); the resulting surface charge of the gold particles was also negative.

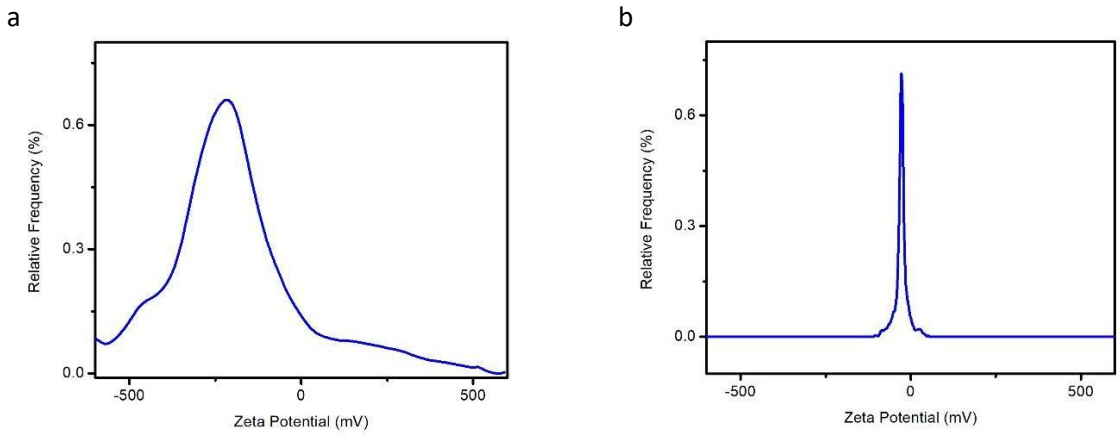

Figure 3.8 (a) The zeta potential of gold was found to be 236 mV, and **(b)** the zeta potential of the liposome was found to be -26 mV.

Since like charges repel each other, it is understood that the negatively charged gold was never truly deposited onto the negatively charged surface of the liposomes, as electrostatic forces would not allow for their bonding.[118] Rengan et al. used a liposome formulation that consisted of DSPC:CHOL in order to yield a positively charged liposome, which allowed the gold particles to attach themselves to the phospholipid bilayer.[87] However, is was still possible to produce positively charged liposomes with the available lipid composition used to make the previous gold-coated liposomes by coating the liposomes with a layer of chitosan prior to the addition of gold.[118] Chitosan is a natural polysaccharide that has been widely used for the development of drug delivery systems, which has the capacity of providing pH-responsive drug release because of its amino groups that can be protonated under acidic conditions.[119] The chitosan can adsorb onto the surface of the negatively charged DPPC:MSPC:PEG-2000 liposomes by electrostatic attraction, inverting the liposome surface charge to positive, and then allow the subsequent deposition and attachment of the negatively charged gold particles.[118] Upon synthesizing these gold-coated liposomes with the mediating chitosan layer, it can be observed from the figure that the surface of the liposomes became blurry because of the chitosan. The gold particles, formed

by reducing chloroauric acid with ascorbic acid, could be obviously observed on the liposome surface, being uniformly distributed on the particle surface. The TEM image in Figure 3.9a shows the expected continuous and compact core-shell structure, and the DLS measurements in 3.9b confirmed that the assembled gold-coated liposomes still have good monodispersity in water, with a polydispersity index of 0.12. Another method of reduction of gold using a sodium borohydride-gold growth solution and ascorbic acid was attempted.[120] This particular method is slow and is called the seed-mediated method. The growth solution consists of gold seeds between 2-5 nm in size.[118] These seeds get deposited onto the surface of the chitosan-coated liposomes and further reduction of gold takes place using ascorbic acid, which yields faster deposition of gold to form the coating.[121] The seed- mediated method increases step by step, and allows for good control of the size and shape, and thus the plasmonic properties, of the gold-coated liposomes. Unfortunately, after several attempts using this method, the synthesis never yielded liposomes with continuous gold shells, but only the gold seeds.[118] The ascorbic acid reduction of gold onto liposomes was favored in this project, and yielded particles shown in Figure 3.7a.

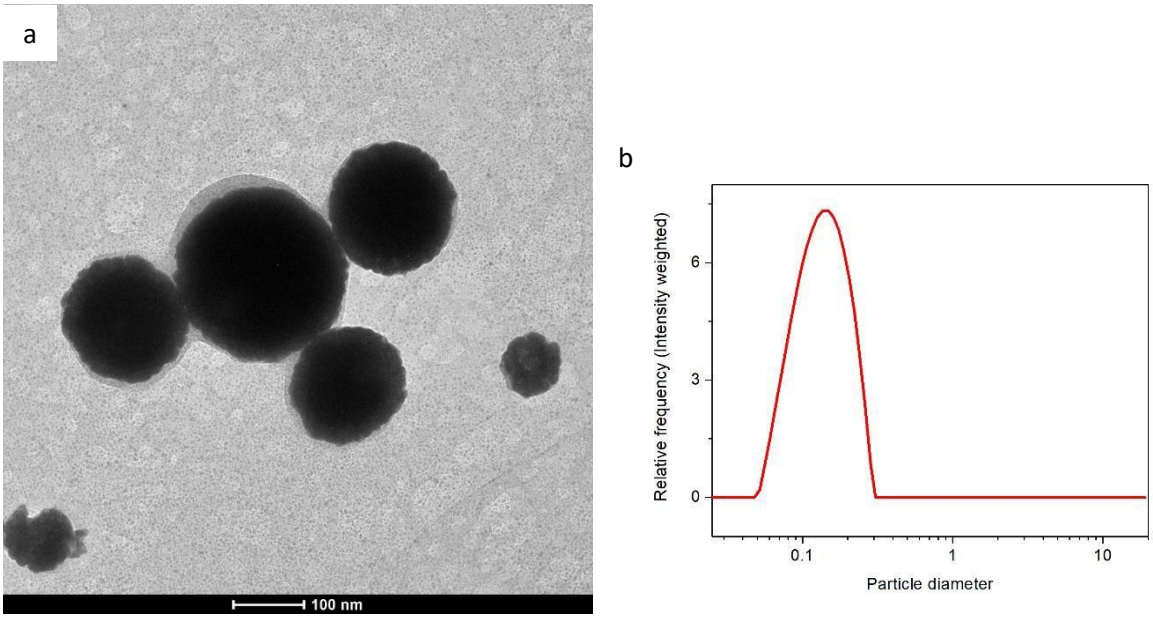

Figure 3.9 (a) TEM image of gold-coated liposome, with the mediating chitosan layer, synthesized using ascorbic acid as the reducing agent. **(b)** DLS measurement depicting the size of the gold coated liposomes to be 140 nm in diameter

It can be noted that the plasmon resonance of these particles is lower than the desired "water window" range. This may be a result of the thickness of the gold shell being too large (plasmon hybridization). In order to obtain a higher plasmon resonance, the gold shell must be made thinner. This was attempted by varying the concentration of gold between 1 and 5 mM in the formulation.

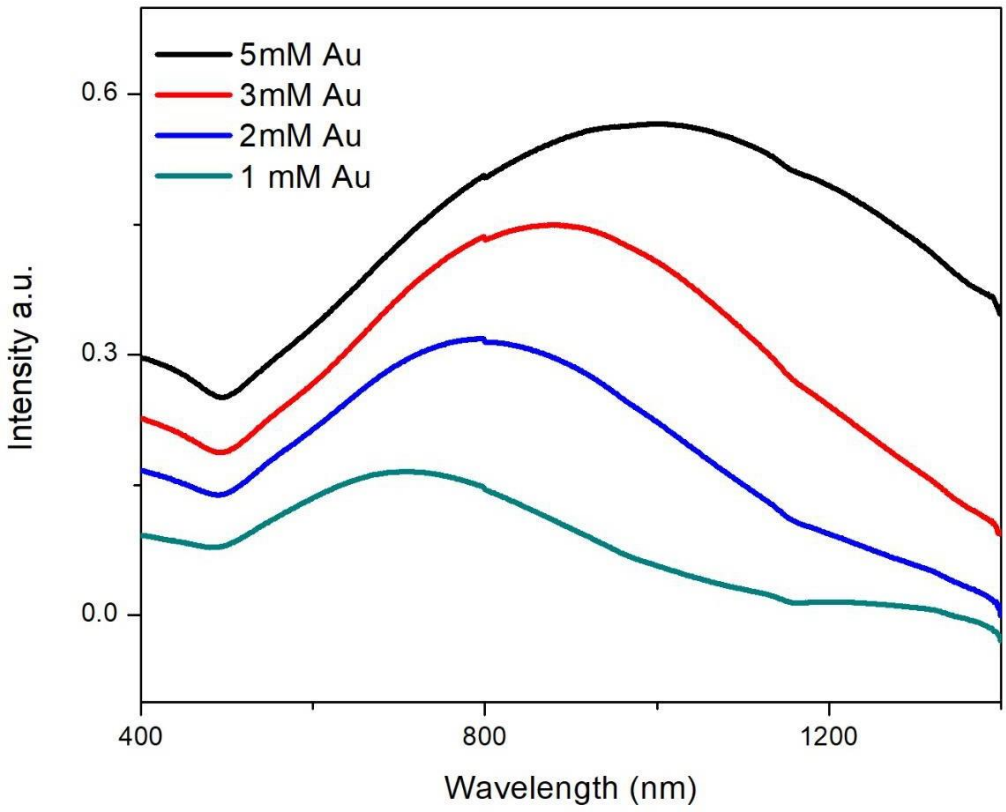

Figure 3.10 Similar to Figure 3.2, the changes in absorption and resonance due to the change in concentration of chloroauric acid; the higher the concentration of chloroauric acid, the greater the red-shift. In staying consistent with the plasmon-hybridization theory, this translates to a higher concentration of gold in the formulation resulting in a thinner shell of gold on the liposome, and hence yielding a higher plasmon resonance.

Figure 3.10 presents the UV-Vis absorption spectra of different liposomes and there were a few absorbance peaks within the NIR region. All the obtained gold-coated liposomes displayed a broad NIR absorbance in the 550-800 nm region, which was beneficial to the application of PTT and also shows that the gold coating was successfully formed. The photothermal conversion capability of the gold-coated liposomes was investigated by monitoring the temperature increase under the irradiation of an 808 nm laser at 2W using an IR camera.

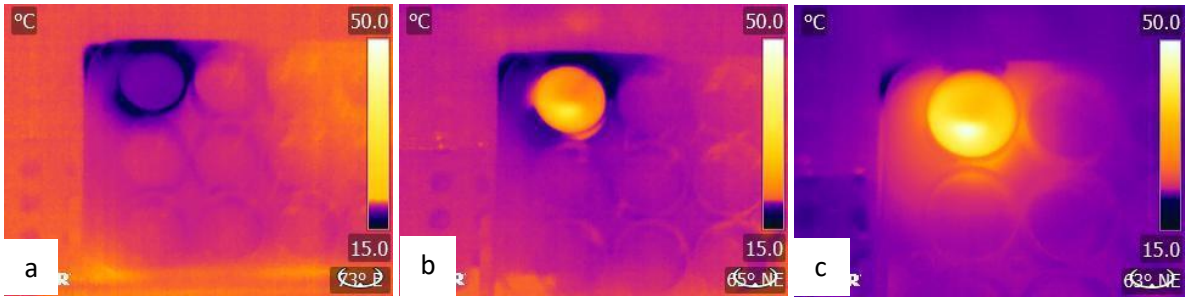

Figure 3.11 (a) irradiated sample at 0 min, (b) irradiated sample at 3 minutes, and (c) irradiated sample at 10 minutes. The longer the sample is irradiated for, the hotter the nanoparticles get. At 10 minutes, the temperature measured using the IR camera was ~46 ºC.

As depicted in Figure 3.11, a rapid temperature elevation in the case of the gold-coated liposomes was observed, where the temperature increased from ambient temperature to 46 ºC within 10 minutes. As mentioned earlier, moderate hyperthermia (41- 43 ºC) was known to be a valid method to inhibit tumor growth and have minimal impact on healthy cells; this phenomenon is due to the fact that tumor cells are more thermally sensitive than normal cells because of poor blood supply and irregular vasculature even with sustained angiogenesis.[122] The photothermal capacity of these particles can be affected by many parameters such as concentration of the nanoparticles, the irradiation power density, etc. The concentration of gold can be determined by using methods such as inductively coupled plasma mass spectrometry (ICP-MS), inductively coupled plasma optical emission spectrometry (ICP-OES) (Figure 3.12), or even thermogravimetric analysis (TGA).[123, 124] It is expected that by increasing the concentration of the particles, and by increasing the power density, one can achieve a higher temperature elevation. These results suggested that the gold-coated liposomes of this formulation can absorb NIR light and convert light energy into heat energy fairly quickly, implying that this formulation containing chitosan holds immense potential for use in photothermal therapy.

Chloroauric Acid Concentration (mM)	Average Concentration of Gold in sample (mg/L)	Standard Deviation
6	10.08	0.25
7	12.00	0.36
8	13.64	0.72
9	14.33	0.37
10	15.35	4.49

Figure 3.12 ICP-OES measurements of gold-coated liposomes. The higher the concentration of chloroauric acid used in the synthesis, the more gold is deposited onto the surface of the liposomes.

3.4 Conclusion

Liposome-gold nanoparticles proved to be efficient candidates for photothermal mediated ablation of cancer. Ascorbic acid deposited gold on the surface of the liposomes optimally, providing a range of plasmon resonances; the gold-coated liposomes' spherical core and sharp protrusions geometry can generate strong nanoantenna effects, and thus amplify the nanostructures' ability to convert light to heat. Thus, the gold-coated liposomes size and shape is favorable for the application of dual modal chemo-photothermal therapy. Earlier, liposomes encapsulated with doxorubicin were synthesized and showed that drug could be released within minutes as the temperature reached and exceeded the phase transition temperature of the liposomes. The resulting nanoparticles' ability to encapsulate drug products within the aqueous core enhances the efficiency of the liposome-gold system, since the combined effort of the photothermal ablation and drug release synergistically improves cancer treatment. However, it is very likely that the gold did not attach to the surface of the liposomes, because the gold particles possessed similar charges. The liposomes that had a mediating layer of chitosan showed great promise in its capacity to encapsulate chemotherapeutic agents like doxorubicin, to fulfill the potential of becoming a photothermal-chemotherapeutic agent for cancer treatment. Future work in this project can include attempts at encapsulating chemotherapeutic drugs, to implement and obtain the synergistic effect of chemotherapy and PTT. The investigations of these effects can be

further explored using *in vitro* models (cancer cell lines to check for cancer treatment activities), and treating these models with varying concentrations of gold-coated liposomes and irradiating with varying power densities of laser light to obtain the optimal combination of usage, as well as to study the cellular uptake of these nanoparticles. The application of such a novel biodegradable hybrid nanoparticle system to cancer nanotherapeutics holds great promise for lowering mortality rates in the future. Cytotoxicity/cell viability can be measured using MTT assay, to aid with determining the optimal concentration and power density. In addition, the synergy therapy, the additive therapeutic efficacies, as well as the independent photothermal treatment and chemotherapeutic treatment can be calculated and studied in order to show the benefits of this new combinative platform. Proliferation and apoptosis assays can be performed to evaluate the therapeutic effect of the designed nanoparticles. Possible experimental designs after optimizing reasonable parameter ranges, include the addition of immunotherapeutic agents while performing animal studies *in vivo,* to study the biodistribution, ablative ability, and targeting capacity, but also to confirm the application of gold-coated liposomes as biocompatible and multifunctional agents for effective cancer treatment, while evaluating normal vs. tumor damage at those high temperatures. Understanding the cellular and molecular basis of the interactions between chemotherapy drugs, the immune system, and photothermal therapy will facilitate the strategic development of this trimodal photochemoimmunotherpay regimen that can maximize the tumor regression, and also the antitumor response for the long term benefit of cancer patients.

3.5 Experimental Methods

Liposomes with a DSPC:MSPC:PEG-2000 molar ratio of 90:10:4 and a total concentration of 2 mg/mL were prepared using the thin film hydration method, in a citrate buffer of pH 4 in order to create an acidic aqueous core for the liposomes. Upon preparing the multi lamellar vesicles

(MLVs), the solution was sonicated for a period of 4.5 min to obtain unilamellar liposomes. The solution was then heated and passed through a series of extrusion syringes with a filter of 100 nm, to obtain a monodisperse solution of liposomes. The buffer in which these liposomes were suspended was then adjusted to have a pH of 7.5, in which doxorubicin was added. Doxorubicin is unprotonated in a pH of 7.5, thus allowing it to diffuse freely across the membrane of the liposome. Once doxorubicin enters the acidic aqueous core, it becomes protonated, in which state it become trapped within and can no longer escape the lipid bilayer, allowing for good biodistribution. Various concentrations of chloroauric acid were added to 20 mM ascorbic acid and 0.4 mg/mL liposomes in a volumetric ratio of 1:4:2, resulting in an abrupt color change from the characteristic cloudy solution of liposomes to shades ranging from dark blue to sea green depending on how much gold was reduced. The solutions were stored in 1.5 mL Eppendorf tubes and attached to a benchtop tube rotator kept at 4 °C. The solutions were mixed for 9 h before taking UV-Vis measurements using the Agilent Cary 60 UV-Vis system. 10 µL of each sample was used for TEM analysis to understand the changes in shape and surface morphology. In order to observe the photothermal capacity of the gold-coated liposomes, ICP-OES was conducted to quantify the concentration of gold that was reduced on the surface of the gold-coated liposomes. The concentrations of these nanostructures in water were varied between 20 and 140 µg/mL, and heated using an 808 nm laser at 5 W/cm^2 for a period of 20 min. This was done to study the appropriate concentration for dosage purposes, in order to achieve mild hyperthermia upon illumination using the 808 nm laser. Time-dependent temperature-triggered doxorubicin release from the gold coated liposomes was studied by placing Eppendorf tubes containing HEPES Buffered Saline (HBS) in a water bath at 37°C. After equilibrating these samples, they were placed in a heating block at two different temperatures - 37°C and 45°C. At time zero, 0.1 mL of the doxorubicn-loaded gold-

coated liposomes at a concentration of 80 µg/mL were added to the HBS solution and incubated for each given time point. De-quenching of doxorubicin fluorescence was monitored at 480 nm. Cumulative DOX release was calculated by,

$$\%\ Dox\ Release = \frac{A_{480\ time\ point} - A_0}{A_\infty - A_0}$$

Where A_0 is the absorbance at time zero, and A_∞ is the absorbance when doxorubicin-loaded gold coated liposomes were lysed by Triton X-100.

To coat the liposomes with chitosan for subsequent coating with gold, 1% chitosan solution was prepared in either 1% ascorbic acid, or 1% acetic acid. To prepare 1% ascorbic acid, 1 g of ascorbic acid was mixed in 99 mL of MilliQ water. To prepare 1% acetic acid, 1 mL of glacial acetic acid was mixed in 99 mL of MilliQ water. Once the 1% acid solutions were prepared, 1 g of chitosan was added to either acid solution in a round-bottomed flask, and a stir-bar was added to the mix, and allowed to mix overnight. Ascorbic acid yielded a more uniform mixture that was easier to filter. A 0.5 mg/mL solution of liposomes was then prepared from the stock solution of liposomes available after extrusion. 5 mL of the 0.5 mg/mL liposome solution was added to a glass vial with a small stir-bar, and the vial was then subsequently placed on a stir-plate. Dropwise, 5 mL of chitosan solution was added to the liposome solution and mixed on a stir-plate for 2 hours, at 500 rpm. After mixing, the solution was stored at 4 ºC.

To coat with gold, two different methods were attempted: ascorbic acid reduction method, or sodium borohydride ($NaBH_4$) seed-mediated method. The ascorbic acid method required the preparation of various concentrations of $HAuCl_4$ (gold salt) – ranging between 1 and 5 mM. 10 µL of 100 mM gold salt was added to 990 µL MilliQ water for 1 mM, and 50 µL of 100 mM gold salt

was added to 950 µL MilliQ water for 5 mM. In order to prepare 20 mM of ascorbic acid in MilliQ water, 35.22 mg of ascorbic acid was added to 10 mL of MilliQ water. To prepare the gold-coated liposomes, the following solutions were mixed in the volumes listed: 100 µL of 1-5mM gold salt solution, 200 µL of 0.5 mg/mL liposome solution, and 400 µL of 20 mM ascorbic acid. The reaction was instantaneous and a color change was observed (transparent to dark green-blue). The plasmon resonance of these particles was directly measured using UV-Vis. The $NaBH_4$ method was a much slower process. 10 µL of 253 mM $NaBH_4$ was mixed with 1 mL of 0.5 mM $AuCl_3$. Both were kept on ice before mixing. This solution was then mixed with liposomes in a 1:3 volume ratio; I mixed 120 µL of gold-seed mixture with 360 µL of liposomes. This mixing took place for 20 hours. Another solution of ice cold 25 µL 20 mM AuCl3 mixed with 975 mL of the thin shelled liposomes was added to 10 µL of $NaBH_4$ and allowed to mix for 8 hours. As mentioned earlier, this reaction is much slower, but yields a similar color change as the ascorbic acid method. I have not had much success with this method, although the particles should have uniform thin gold shells according to literature.

CHAPTER 4

SUMMARY AND OUTLOOK

Overall in this work, tunable gold nanostars and gold-coated liposomes were synthesized with plasmon resonances within the desired NIR range. We were able to functionalize the gold nanostars with antigen-specific peptides and Raman reporter tags, demonstrating the maneuverability and versatility of the nanostructures. We incorporated these gold nanostars as detection probes for an ultrasensitive sandwich diagnostic assay that allowed for SERS mediated sensing of protein analytes. A detection limit of 30 pg/mL of cardiac troponin I (cTnI) was achieved in buffer solution, indicating the high sensitivity achieved by this assay to detect concentrations within the gray zone of clinical concern. These initial tests served as proof of concept studies, envisioning a biodiagnostic tool for the early detection of a myocardial infarction through blood or serum analysis of cTnI levels. In order to test the robustness and sensitivity of the assay using biological fluids, deidentified serum that was spiked with different concentrations of cTnI was used, and yielded results that demonstrated potential for a more sophisticated diagnostic tool. To establish a truly rapid and reusable substrate for future biomolecular SERS detection, the incorporation of a single planar yet flexible substrate, with an intricate mixing channel, would be beneficial.

The ability to develop gold-coated liposomes with intense photothermal efficiencies, raising the surrounding temperatures to ~46 ºC within 10 minutes of illumination, shows great potential for novel cancer therapies. The tunability of these particles to have plasmon resonances within the first NIR range, serves as a platform for future *in vivo* therapeutic studies. The hollow cavity of the coated liposomes can potentially allow for the stable encapsulation of chemotherapeutic drugs to enable effective synergistic chemo-photothermal therapy. In the future,

the surface of the gold-coated liposomes can also be functionalized with antibodies to recognize overexpressed proteins/receptors on specific tumor cells, to make for a more efficient therapeutic platform that relies on active targeting of the cancers, instead of passive targeting which entails largely the EPR effect. This engineered platform can also be further improved by adding an imaging modality to it, to serve the dual purpose of detecting as well as treating cancers. Since the surface of gold is easy to modify, fluorescent tags for biomolecular imaging purposes can possibly be attached to these gold-coated liposomes, to make them a true theranostic platform.[125] In another ambitious effort, these gold-coated liposomes can possibly be coupled with immunotherapeutic or immunomodulatory agents, upon administration for the treatment of aggressive cancers that can potentially benefit from the photochemoimmuno-therapeutic effect of the platform.[126]

The work presented here demonstrates the versatile and conformable potential of synthesized gold nanoparticles to provide a quantitative measure of bioanalytes and also to allow for potential personalized image-guided photochemoimmunotherapy with reduced toxicity. These nanoplatforms can be further studied to eventually develop viable multifunctional tools that can translate to practical and applicable individualized nanomedicine.

REFERENCES

1. Masoudkabir, F., et al., *Cardiovascular disease and cancer: Evidence for shared disease pathways and pharmacologic prevention.* Atherosclerosis, 2017. **263**: p. 343-351.
2. Long, H.D., et al., *Risk of Congestive Heart Failure in Early Breast Cancer Patients Undergoing Adjuvant Treatment With Trastuzumab: A Meta-Analysis.* Oncologist, 2016. **21**(5): p. 547-54.
3. Blaes, A., et al., *Cardio-oncology Related to Heart Failure: Common Risk Factors Between Cancer and Cardiovascular Disease.* Heart Fail Clin, 2017. **13**(2): p. 367-380.
4. Patil, M., D.S. Mehta, and S. Guvva, *Future impact of nanotechnology on medicine and dentistry.* J Indian Soc Periodontol, 2008. **12**(2): p. 34-40.
5. Singh, R. and J.W. Lillard, Jr., *Nanoparticle-based targeted drug delivery.* Exp Mol Pathol, 2009. **86**(3): p. 215-23.
6. Hornos Carneiro, M.F. and F. Barbosa, Jr., *Gold nanoparticles: A critical review of therapeutic applications and toxicological aspects.* J Toxicol Environ Health B Crit Rev, 2016. **19**(3-4): p. 129-48.
7. Chinen, A.B., et al., *Nanoparticle Probes for the Detection of Cancer Biomarkers, Cells, and Tissues by Fluorescence.* Chem Rev, 2015. **115**(19): p. 10530-74.
8. Dreaden, E.C., et al., *Size matters: gold nanoparticles in targeted cancer drug delivery.* Ther Deliv, 2012. **3**(4): p. 457-78.
9. Riley, R.S. and E.S. Day, *Gold nanoparticle-mediated photothermal therapy: applications and opportunities for multimodal cancer treatment.* Wiley Interdiscip Rev Nanomed Nanobiotechnol, 2017. **9**(4).
10. Moore, T.J., et al., *In Vitro and In Vivo SERS Biosensing for Disease Diagnosis.* Biosensors (Basel), 2018. **8**(2).
11. Carter, D., *New global survey shows an increasing cancer burden.* Am J Nurs, 2014. **114**(3): p. 17.
12. Koene, R.J., et al., *Shared Risk Factors in Cardiovascular Disease and Cancer.* Circulation, 2016. **133**(11): p. 1104-14.
13. Krakhmal, N.V., et al., *Cancer Invasion: Patterns and Mechanisms.* Acta Naturae, 2015. **7**(2): p. 17-28.
14. Strohmeyer, T.G. and D.J. Slamon, *Proto-oncogenes and tumor suppressor genes in human urological malignancies.* J Urol, 1994. **151**(6): p. 1479-97.
15. Hanahan, D. and R.A. Weinberg, *Hallmarks of cancer: the next generation.* Cell, 2011. **144**(5): p. 646-74.
16. Hainaut, P. and A. Plymoth, *Targeting the hallmarks of cancer: towards a rational approach to next-generation cancer therapy.* Curr Opin Oncol, 2013. **25**(1): p. 50-1.
17. Tenga, M.J. and I.M. Lazar, *Proteomic snapshot of breast cancer cell cycle: G1/S transition point.* Proteomics, 2013. **13**(1): p. 48-60.
18. Austin, L.A., et al., *The optical, photothermal, and facile surface chemical properties of gold and silver nanoparticles in biodiagnostics, therapy, and drug delivery.* Arch Toxicol, 2014. **88**(7): p. 1391-417.
19. Zhang, Y., H. Hong, and W. Cai, *Imaging with Raman spectroscopy.* Curr Pharm Biotechnol, 2010. **11**(6): p. 654-61.
20. Gonzalez-Solis, J., G. Luevano-Colmenero, and J. Vargas-Mancilla, *Surface enhanced Raman spectroscopy in breast cancer cells.* Laser Ther, 2013. **22**(1): p. 37-42.
21. Li, M., S.K. Cushing, and N. Wu, *Plasmon-enhanced optical sensors: a review.* Analyst, 2015.

140(2): p. 386-406.
22. Israelsen, N.D., C. Hanson, and E. Vargis, *Nanoparticle properties and synthesis effects on surface-enhanced Raman scattering enhancement factor: an introduction.* ScientificWorldJournal, 2015. **2015**: p. 124582.
23. Smolsky, J., et al., *Surface-Enhanced Raman Scattering-Based Immunoassay Technologies for Detection of Disease Biomarkers.* Biosensors (Basel), 2017. **7**(1).
24. Abalde-Cela, S., et al., *Surface-enhanced Raman scattering biomedical applications of plasmonic colloidal particles.* J R Soc Interface, 2010. **7 Suppl 4**: p. S435-50.
25. Wang, J., et al., *Surface Plasmon Resonance Sensors on Raman and Fluorescence Spectroscopy.* Sensors (Basel), 2017. **17**(12).
26. Khoury, C.G. and T. Vo-Dinh, *Gold Nanostars For Surface-Enhanced Raman Scattering: Synthesis, Characterization and Optimization.* J Phys Chem C Nanomater Interfaces, 2008. **2008**(112): p. 18849-18859.
27. Sinha, S.S., et al., *Nanoarchitecture Based SERS for Biomolecular Fingerprinting and Label-Free Disease Markers Diagnosis.* Acc Chem Res, 2016. **49**(12): p. 2725-2735.
28. Yeo, B.S., et al., *A strategy to prevent signal losses, analyte decomposition, and fluctuating carbon contamination bands in surface-enhanced Raman spectroscopy.* Appl Spectrosc, 2008. **62**(6): p. 708-13.
29. Ravanshad, R., et al., *Application of nanoparticles in cancer detection by Raman scattering based techniques.* Nano Rev Exp, 2018. **9**(1): p. 1373551.
30. D'Hollander, A., et al., *Development of nanostars as a biocompatible tumor contrast agent: toward in vivo SERS imaging.* Int J Nanomedicine, 2016. **11**: p. 3703-14.
31. Navas-Moreno, M., et al., *Nanoparticles for live cell microscopy: A surface-enhanced Raman scattering perspective.* Sci Rep, 2017. **7**(1): p. 4471.
32. Olson, J., et al., *Optical characterization of single plasmonic nanoparticles.* Chem Soc Rev, 2015. **44**(1): p. 40-57.
33. D'Acunto, M., *Detection of Intracellular Gold Nanoparticles: An Overview.* Materials (Basel), 2018. **11**(6).
34. Chatterjee, D.K., P. Diagaradjane, and S. Krishnan, *Nanoparticle-mediated hyperthermia in cancer therapy.* Ther Deliv, 2011. **2**(8): p. 1001-14.
35. Vriend, L.E.M., et al., *Boosting the effects of hyperthermia-based anticancer treatments by HSP90 inhibition.* Oncotarget, 2017. **8**(57): p. 97490-97503.
36. Knavel, E.M. and C.L. Brace, *Tumor ablation: common modalities and general practices.* Tech Vasc Interv Radiol, 2013. **16**(4): p. 192-200.
37. Ahmed, M., et al., *Image-guided tumor ablation: standardization of terminology and reporting criteria--a 10-year update.* J Vasc Interv Radiol, 2014. **25**(11): p. 1691-705 e4.
38. Vo-Dinh, T., H.N. Wang, and J. Scaffidi, *Plasmonic nanoprobes for SERS biosensing and bioimaging.* J Biophotonics, 2010. **3**(1-2): p. 89-102.
39. Granger, J.H., et al., *Prospects for point-of-care pathogen diagnostics using surface-enhanced Raman scattering (SERS).* Chem Soc Rev, 2016. **45**(14): p. 3865-82.
40. Tsoutsi, D., et al., *Common Aspects Influencing the Translocation of SERS to Biomedicine.* Curr Med Chem, 2018. **25**(35): p. 4638-4652.
41. Wu, L., et al., *Simultaneous evaluation of p53 and p21 expression level for early cancer diagnosis using SERS technique.* Analyst, 2013. **138**(12): p. 3450-6.
42. Li, M., et al., *Three-dimensional hierarchical plasmonic nano-architecture enhanced surface-enhanced Raman scattering immunosensor for cancer biomarker detection in blood plasma.* ACS

Nano, 2013. **7**(6): p. 4967-76.
43. Romeo, A., T.S. Leung, and S. Sanchez, *Smart biosensors for multiplexed and fully integrated point-of-care diagnostics.* Lab Chip, 2016. **16**(11): p. 1957-61.
44. Dincer, C., et al., *Multiplexed Point-of-Care Testing - xPOCT.* Trends Biotechnol, 2017. **35**(8): p. 728-742.
45. Masson, J.F., *Surface Plasmon Resonance Clinical Biosensors for Medical Diagnostics.* ACS Sens, 2017. **2**(1): p. 16-30.
46. Wang, R., et al., *Highly Sensitive Detection of Hormone Estradiol E2 Using Surface-Enhanced Raman Scattering Based Immunoassays for the Clinical Diagnosis of Precocious Puberty.* ACS Appl Mater Interfaces, 2016. **8**(17): p. 10665-72.
47. Chen, P., et al., *Multiplex serum cytokine immunoassay using nanoplasmonic biosensor microarrays.* ACS Nano, 2015. **9**(4): p. 4173-81.
48. Luan, J., et al., *Add-on plasmonic patch as a universal fluorescence enhancer.* Light Sci Appl, 2018. **7**: p. 29.
49. Polavarapu, L. and L.M. Liz-Marzan, *Towards low-cost flexible substrates for nanoplasmonic sensing.* Phys Chem Chem Phys, 2013. **15**(15): p. 5288-300.
50. Shen, L., J.A. Hagen, and I. Papautsky, *Point-of-care colorimetric detection with a smartphone.* Lab Chip, 2012. **12**(21): p. 4240-3.
51. Wan, Y., et al., *Development of electrochemical immunosensors towards point of care diagnostics.* Biosens Bioelectron, 2013. **47**: p. 1-11.
52. Rogers, M.L. and M.G. Boutelle, *Real-time clinical monitoring of biomolecules.* Annu Rev Anal Chem (Palo Alto Calif), 2013. **6**: p. 427-53.
53. Perkel, J.M., *Pocket laboratories.* Nature, 2017. **545**(7652): p. 119-121.
54. Cheng, Z., et al., *Simultaneous Detection of Dual Prostate Specific Antigens Using Surface-Enhanced Raman Scattering-Based Immunoassay for Accurate Diagnosis of Prostate Cancer.* ACS Nano, 2017. **11**(5): p. 4926-4933.
55. Kang, H., et al., *Direct Identification of On-Bead Peptides Using Surface-Enhanced Raman Spectroscopic Barcoding System for High-Throughput Bioanalysis (vol 5, 10144, 2015).* Scientific Reports, 2015. **5**.
56. Polavarapu, L., et al., *Pen-on-paper approach toward the design of universal surface enhanced Raman scattering substrates.* Small, 2014. **10**(15): p. 3065-71.
57. Wang, Z., et al., *SERS-Activated Platforms for Immunoassay: Probes, Encoding Methods, and Applications.* Chem Rev, 2017. **117**(12): p. 7910-7963.
58. Webb, J.A. and R. Bardhan, *Emerging advances in nanomedicine with engineered gold nanostructures.* Nanoscale, 2014. **6**(5): p. 2502-30.
59. Ou, Y.C., et al., *Gold Nanoantenna-Mediated Photothermal Drug Delivery from Thermosensitive Liposomes in Breast Cancer.* ACS Omega, 2016. **1**(2): p. 234-243.
60. Webb, J.A., et al., *Geometry-Dependent Plasmonic Tunability and Photothermal Characteristics of Multibranched Gold Nanoantennas.* The Journal of Physical Chemistry C, 2014. **118**(7): p. 3696-3707.
61. Ou, Y.C., et al., *Diagnosis of immunomarkers in vivo via multiplexed surface enhanced Raman spectroscopy with gold nanostars.* Nanoscale, 2018. **10**(27): p. 13092-13105.
62. Webb, J.A., et al., *Theranostic Gold Nanoantennas for Simultaneous Multiplexed Raman Imaging of Immunomarkers and Photothermal Therapy.* ACS Omega, 2017. **2**(7): p. 3583-3594.
63. Sandhu, R., et al., *Relation of cardiac troponin I levels with in-hospital mortality in patients with ischemic stroke, intracerebral hemorrhage, and subarachnoid hemorrhage.* Am J Cardiol, 2008.

102(5): p. 632-4.
64. Mahajan, V.S. and P. Jarolim, *How to interpret elevated cardiac troponin levels.* Circulation, 2011. **124**(21): p. 2350-4.
65. Kuang, Z., et al., *Biomimetic chemosensor: designing peptide recognition elements for surface functionalization of carbon nanotube field effect transistors.* ACS Nano, 2010. **4**(1): p. 452-8.
66. Tadepalli, S., et al., *Peptide Functionalized Gold Nanorods for the Sensitive Detection of a Cardiac Biomarker Using Plasmonic Paper Devices.* Sci. Rep., 2015. **5**: p. 16206.
67. Enman, N.M., et al., *Targeting the Neuropeptide Y System in Stress-related Psychiatric Disorders.* Neurobiol Stress, 2015. **1**: p. 33-43.
68. Sah, R. and T.D. Geracioti, *Neuropeptide Y and posttraumatic stress disorder.* Mol Psychiatry, 2013. **18**(6): p. 646-55.
69. Morgan, C.A., 3rd, et al., *Plasma neuropeptide-Y concentrations in humans exposed to military survival training.* Biol Psychiatry, 2000. **47**(10): p. 902-9.
70. Yeh, E.C., et al., *Self-powered integrated microfluidic point-of-care low-cost enabling (SIMPLE) chip.* Sci Adv, 2017. **3**(3): p. e1501645.
71. Mark, D., et al., *Microfluidic lab-on-a-chip platforms: requirements, characteristics and applications.* Chem Soc Rev, 2010. **39**(3): p. 1153-82.
72. Murdock, R.C., et al., *Optimization of a paper-based ELISA for a human performance biomarker.* Anal Chem, 2013. **85**(23): p. 11634-42.
73. Tadepalli, S., et al., *Peptide Functionalized Gold Nanorods for the Sensitive Detection of a Cardiac Biomarker Using Plasmonic Paper Devices.* Sci Rep, 2015. **5**: p. 16206.
74. Xiao, X., et al., *Advancing Peptide-Based Biorecognition Elements for Biosensors Using in-Silico Evolution.* ACS Sens, 2018. **3**(5): p. 1024-1031.
75. Wang, C., et al., *Polyethylenimine-interlayered core-shell-satellite 3D magnetic microspheres as versatile SERS substrates.* Nanoscale, 2015. **7**(44): p. 18694-707.
76. Psychogios, N., et al., *The Human Serum Metabolome.* PLoS ONE, 2011. **6**(2): p. e16957.
77. Bonifacio, A., S. Cervo, and V. Sergo, *Label-free surface-enhanced Raman spectroscopy of biofluids: fundamental aspects and diagnostic applications.* Anal Bioanal Chem, 2015. **407**(27): p. 8265-77.
78. Zhang, X., et al., *A simple microfluidic platform for rapid and efficient production of the radiotracer [(18)F]fallypride.* Lab Chip, 2018. **18**(9): p. 1369-1377.
79. Goode, J.A., J.V. Rushworth, and P.A. Millner, *Biosensor Regeneration: A Review of Common Techniques and Outcomes.* Langmuir, 2015. **31**(23): p. 6267-76.
80. Drake, A.W. and S.L. Klakamp, *A strategic and systematic approach for the determination of biosensor regeneration conditions.* J Immunol Methods, 2011. **371**(1-2): p. 165-9.
81. Wikstrom, M.B., et al., *Degradation of human immunoglobulins by proteases from Streptococcus pneumoniae obtained from various human sources.* Infect Immun, 1984. **44**(1): p. 33-7.
82. Di Angelantonio, E., et al., *Prognostic significance of admission levels of troponin I in patients with acute ischaemic stroke.* J. Neurol. Neurosurg. Psychiatry, 2005. **76**(1): p. 76-81.
83. Fletcher, M.A., et al., *Plasma neuropeptide Y: a biomarker for symptom severity in chronic fatigue syndrome.* Behav. Brain. Funct., 2010. **6**: p. 76.
84. Scirica, B.M. and D.A. Morrow, *Troponins in acute coronary syndromes.* Progress in Cardiovascular Diseases, 2004. **47**(3): p. 177-188.
85. Temiz, Y. and E. Delamarche, *Sub-nanoliter, real-time flow monitoring in microfluidic chips using a portable device and smartphone.* Scientific Reports, 2018. **8**.
86. Giljohann, D.A., et al., *Gold nanoparticles for biology and medicine.* Angew Chem Int Ed Engl,

2010. **49**(19): p. 3280-94.
87. Rengan, A.K., et al., *In vivo analysis of biodegradable liposome gold nanoparticles as efficient agents for photothermal therapy of cancer.* Nano Lett, 2015. **15**(2): p. 842-8.
88. Cai, W., et al., *Applications of gold nanoparticles in cancer nanotechnology.* Nanotechnol Sci Appl, 2008. **1**: p. 17-32.
89. Jain, S., D.G. Hirst, and J.M. O'Sullivan, *Gold nanoparticles as novel agents for cancer therapy.* Br J Radiol, 2012. **85**(1010): p. 101-13.
90. Xu, J., et al., *Renal clearable noble metal nanoparticles: photoluminescence, elimination, and biomedical applications.* Wiley Interdiscip Rev Nanomed Nanobiotechnol, 2017. **9**(5).
91. Leung, S.J., T.S. Troutman, and M. Romanowski, *Plasmon resonant gold-coated liposomes for spectrally coded content release.* Proc SPIE Int Soc Opt Eng, 2009. **7190**.
92. Troutman, T.S., J.K. Barton, and M. Romanowski, *Biodegradable Plasmon Resonant Nanoshells.* Adv Mater, 2008. **20**(13): p. 2604-2608.
93. Mathiyazhakan, M., C. Wiraja, and C. Xu, *A Concise Review of Gold Nanoparticles-Based Photo-Responsive Liposomes for Controlled Drug Delivery.* Nanomicro Lett, 2018. **10**(1): p. 10.
94. Puri, A., et al., *Lipid-based nanoparticles as pharmaceutical drug carriers: from concepts to clinic.* Crit Rev Ther Drug Carrier Syst, 2009. **26**(6): p. 523-80.
95. Youssefian, S., et al., *Variation of thermal conductivity of DPPC lipid bilayer membranes around the phase transition temperature.* J R Soc Interface, 2017. **14**(130).
96. Huang, H.C., K. Rege, and J.J. Heys, *Spatiotemporal temperature distribution and cancer cell death in response to extracellular hyperthermia induced by gold nanorods.* ACS Nano, 2010. **4**(5): p. 2892-900.
97. Arruebo, M., et al., *Assessment of the evolution of cancer treatment therapies.* Cancers (Basel), 2011. **3**(3): p. 3279-330.
98. Crawford, S., *Is it time for a new paradigm for systemic cancer treatment? Lessons from a century of cancer chemotherapy.* Front Pharmacol, 2013. **4**: p. 68.
99. Luo, D., et al., *Doxorubicin encapsulated in stealth liposomes conferred with light-triggered drug release.* Biomaterials, 2016. **75**: p. 193-202.
100. Xing, M., et al., *Efficacy and Cardiotoxicity of Liposomal Doxorubicin-Based Chemotherapy in Advanced Breast Cancer: A Meta-Analysis of Ten Randomized Controlled Trials.* PLoS One, 2015. **10**(7): p. e0133569.
101. Hendry, S.A., et al., *The Role of the Tumor Vasculature in the Host Immune Response: Implications for Therapeutic Strategies Targeting the Tumor Microenvironment.* Front Immunol, 2016. **7**: p. 621.
102. Rosenblum, D., et al., *Progress and challenges towards targeted delivery of cancer therapeutics.* Nat Commun, 2018. **9**(1): p. 1410.
103. Linsley, C.S. and B.M. Wu, *Recent advances in light-responsive on-demand drug-delivery systems.* Ther Deliv, 2017. **8**(2): p. 89-107.
104. Knights-Mitchell, S.S. and M. Romanowski, *Near-Infrared Activated Release of Doxorubicin from Plasmon Resonant Liposomes.* Nanotheranostics, 2018. **2**(4): p. 295-305.
105. Pradhan, P., et al., *Targeted Magnetic Liposomes Loaded with Doxorubicin.* Methods Mol Biol, 2017. **1522**: p. 257-272.
106. Park, S.M., et al., *Novel temperature-triggered liposome with high stability: formulation, in vitro evaluation, and in vivo study combined with high-intensity focused ultrasound (HIFU).* J Control Release, 2013. **170**(3): p. 373-9.
107. Ringe, E., et al., *Correlating the structure and localized surface plasmon resonance of single silver*

right bipyramids. Nanotechnology, 2012. **23**(44): p. 444005.
108. Peng, S., et al., *Reversing the size-dependence of surface plasmon resonances.* Proc Natl Acad Sci U S A, 2010. **107**(33): p. 14530-4.
109. Rahman, A.M., S.W. Yusuf, and M.S. Ewer, *Anthracycline-induced cardiotoxicity and the cardiac-sparing effect of liposomal formulation.* Int J Nanomedicine, 2007. **2**(4): p. 567-83.
110. Bozzuto, G. and A. Molinari, *Liposomes as nanomedical devices.* Int J Nanomedicine, 2015. **10**: p. 975-99.
111. Hu, Y., R.C. Fleming, and R.A. Drezek, *Optical properties of gold-silica-gold multilayer nanoshells.* Opt Express, 2008. **16**(24): p. 19579-91.
112. Shi, W., et al., *Gold nanoshells on polystyrene cores for control of surface plasmon resonance.* Langmuir, 2005. **21**(4): p. 1610-7.
113. Prevo, B.G., et al., *Scalable routes to gold nanoshells with tunable sizes and response to near-infrared pulsed-laser irradiation.* Small, 2008. **4**(8): p. 1183-95.
114. De Carlo, S. and J.R. Harris, *Negative staining and cryo-negative staining of macromolecules and viruses for TEM.* Micron, 2011. **42**(2): p. 117-31.
115. Drulyte, I., et al., *Approaches to altering particle distributions in cryo-electron microscopy sample preparation.* Acta Crystallogr D Struct Biol, 2018. **74**(Pt 6): p. 560-571.
116. Cheng, Y., et al., *A primer to single-particle cryo-electron microscopy.* Cell, 2015. **161**(3): p. 438-449.
117. Alinaghi, A., et al., *The influence of lipid composition and surface charge on biodistribution of intact liposomes releasing from hydrogel-embedded vesicles.* Int J Pharm, 2014. **459**(1-2): p. 30-9.
118. Wang M., L.Y., Zhang X., Luo L., Li L., Xing S., He Y., Cao W., Zhu R., Gao D, *Gold Nanoshell Coated thermo-pH Dual Responsive Liposomes for Resveratrol Delivery and Chemo-Photothermal Synergistic Cancer Therapy.* J. Mater. Chem. B., 2017. **5**: p. 2161-2171.
119. Cheung, R.C., et al., *Chitosan: An Update on Potential Biomedical and Pharmaceutical Applications.* Mar Drugs, 2015. **13**(8): p. 5156-86.
120. Kohout, C., C. Santi, and L. Polito, *Anisotropic Gold Nanoparticles in Biomedical Applications.* Int J Mol Sci, 2018. **19**(11).
121. Freitas de Freitas, L., et al., *An Overview of the Synthesis of Gold Nanoparticles Using Radiation Technologies.* Nanomaterials (Basel), 2018. **8**(11).
122. Yan, G., et al., *Polymer-Based Nanocarriers for Co-Delivery and Combination of Diverse Therapies against Cancers.* Nanomaterials (Basel), 2018. **8**(2).
123. Elci, S.G., et al., *Quantitative imaging of 2 nm monolayer-protected gold nanoparticle distributions in tissues using laser ablation inductively-coupled plasma mass spectrometry (LA-ICP-MS).* Analyst, 2016. **141**(8): p. 2418-25.
124. Sebby, K.B. and E. Mansfield, *Determination of the surface density of polyethylene glycol on gold nanoparticles by use of microscale thermogravimetric analysis.* Anal Bioanal Chem, 2015. **407**(10): p. 2913-22.
125. Andreou, C., et al., *Molecular Imaging in Nanotechnology and Theranostics.* Mol Imaging Biol, 2017. **19**(3): p. 363-372.
126. Milling, L., Y. Zhang, and D.J. Irvine, *Delivering safer immunotherapies for cancer.* Adv Drug Deliv Rev, 2017. **114**: p. 79-101.